HHS Public Access

Author manuscript

Nat Immunol. Author manuscript; available in PMC 2020 May 25.

Published in final edited form as:

Nat Immunol. 2020 January ; 21(1): 42–53. doi:10.1038/s41590-019-0539-2.

Endogenous oxidized phospholipids reprogram cellular metabolism and boost hyperinflammation

Marco Di Gioia[1], **Roberto Spreafico**[2], **James R. Springstead**[3], **Michael M. Mendelson**[4], **Roby Joehanes**[5], **Daniel Levy**[5], **Ivan Zanoni**[1,6]

[1]Harvard Medical School and Boston Children's Hospital, Division of Immunology and Division of Gastroenterology, Boston, Massachusetts, USA.

[2]Institute for Quantitative and Computational Biosciences, University of California, Los Angeles, California, USA.

[3]Department of Chemical and Paper Engineering, Western Michigan University, Kalamazoo, Michigan, USA.

[4]Department of Cardiology, Boston Children's Hospital, Boston, Massachusetts, USA.

[5]Population Sciences Branch, Division of Intramural Research, National Heart, Lung, and Blood Institute, National Institutes of Health, Bethesda, MD, USA.

[6]Department of Biotechnology and Biosciences, University of Milano - Bicocca, Milan, Italy.

Abstract

Pathogen-associated molecular patterns (PAMPs) have the capacity to couple inflammatory gene expression to changes in macrophage metabolism, both of which influence subsequent inflammatory activities. Similar to their microbial counterparts, several self-encoded damage-associated molecular patterns (DAMPs) induce inflammatory gene expression. However, whether this symmetry in host responses between PAMPs and DAMPs extends to metabolic shifts is unclear. Here we report that the self-encoded oxidized phospholipid oxPAPC alters the metabolism of macrophages exposed to lipopolysaccharide (LPS). While cells activated by LPS rely exclusively on glycolysis, macrophages exposed to oxPAPC also use mitochondrial respiration, feed the Krebs cycle with glutamine and favor the accumulation of oxaloacetate in the cytoplasm: this metabolite potentiates IL-1β production, resulting in hyperinflammation. Similar metabolic adaptions occur *in vivo* in hypercholesterolemic mice and human subjects. Drugs that interfere with oxPAPC-driven metabolic changes reduce atherosclerotic plaque formation in mice, thereby underscoring the importance of DAMP-mediated activities in pathophysiological conditions.

Correspondence: ivan.zanoni@childrens.harvard.edu.

AUTHOR CONTRIBUTION

MDG designed, performed and analyzed the experiments; RS performed the statistical comparisons on the FHS aggregated data; JRS produced oxPAPC and PEIPC and participated to the analyses of data; MMM, RJ, and DL developed and analyzed the FHS expression project; IZ conceived the project, designed the experiments, supervised the study and wrote the paper.

COMPETING INTERESTS:

IZ, MDG and Boston Children's Hospital have filed an international patent application (US62/851,561) that relates to the metabolic activity of oxPAPC.

INTRODUCTION

Inflammation protects against sterile as well as microbial injuries. Our understanding of factors that drive the development of inflammation is based on the activity of pattern recognition receptors (PRRs)[1]. These receptors detect pathogen-associated molecular patterns (PAMPs)[2] and self molecules known as damage-associated molecular patterns (DAMPs)[3]. Development of a proper inflammatory response likely require the coincident recognition of PAMPs and DAMPs[4, 5].

A class of DAMPs that is represented by oxidized phospholipids, derived from 1-palmitoyl-2-arachidonyl-*sn*-glycero-3-phosphorylcholine (PAPC) (collectively known as oxPAPC), functions together with PAMPs to elicit maximal immune responses[6, 7]. oxPAPC is produced at the site of infectious as well as non-infectious tissue injury[8, 9, 10, 11, 12], and is also an active component of the oxidized low density lipoprotein (oxLDL) aggregate that promotes atherosclerosis[13, 14]. In the presence of the lipopolysaccharide (LPS) that forms the cell wall of Gram-negative bacteria, selected moieties (e.g., POVPC and PGPC) present in the oxPAPC mixture potently induce a form of inflammasome activation, which leads to the secretion of interleukin (IL)-1β, a key inflammatory mediator[15], but prevents pyroptosis and favors phagocyte survival[6, 7]. We thus refer to oxPAPC as a vita-DAMP that induces a “hyperactivated” state in phagocytes and potentiates the inflammatory response.

Phagocytes treated with LPS encounter metabolic changes that dictate the production of inflammatory mediators[16]. While resting phagocytes rely predominantly on mitochondria-driven oxidative phosphorylation (OXPHOS), cells that are stimulated with LPS undergo a rapid metabolic shift to aerobic glycolysis[17]. The glycolytic shift provides ATP, feeds the pentose phosphate pathway (PPP), and generates pyruvate to fuel the Krebs, or tricarboxylic acid (TCA), cycle that is broken after LPS stimulation[18]. Whether a self-moiety such as oxPAPC that is able to sustain the lifespan and to potentiate the inflammatory activity of phagocytes achieves this by altering the metabolic switch driven by LPS remains largely overlooked.

Here we report that oxPAPC potently boosts the production of IL-1β by rewiring the metabolism of macrophages stimulated with LPS. We show that similar immunometabolic adaptations occur *in vivo* in atherosclerotic mice, and drugs that interfere with oxPAPC-driven metabolic changes reduce atherosclerotic plaque formation. Furthermore, complementary transcriptional changes associated with the metabolic state induced by oxPAPC also occur in the blood of hypercholesterolemic community-dwelling adults. Overall, our findings demonstrate that oxPAPC boosts inflammation, not merely by driving the formation of “hyperactive” cells that are characterized by inflammasome activation in the absence of pyroptosis[6, 7], but also by engaging a “hypermetabolic” state in phagocytes that boosts the production of IL-1β.

RESULTS

Endogenous oxidized lipids promote simultaneous OXPHOS and aerobic glycolysis in LPS-stimulated phagocytes.

To mimic a threatening condition in which an initial encounter with a pathogen is followed by tissue damage, macrophage colony stimulating factor (M-CSF) bone marrow-derived macrophages were primed with LPS, and then treated with oxPAPC. To ascertain the metabolic state of cells, we evaluated the oxygen consumption rate (OCR) as a measure of mitochondrial respiration, and the extracellular acidification rate (ECAR) to assess glycolytic flux. As reported[19], the OCR was significantly inhibited and ATP-coupled respiration was almost completely nullified, while ECAR was elevated, in response to LPS relative to untreated macrophages (Fig. 1a, b). Exposure to oxPAPC alone led to a slight increase in the glycolytic flux as well as in the basal OCR (Fig. 1a, b), as reported for macrophages exposed to oxidized phospholipids that reside in the adipose tissue[20]. However, the metabolic profile of the phagocytes exposed to LPS plus oxPAPC was substantially altered: the level of OXPHOS was similar to that in untreated cells, ECAR was elevated as in cells treated with LPS only, and ATP-coupled respiration was potently boosted in cells exposed to LPS and oxPAPC, relative to macrophages treated with LPS only. (Fig. 1a, b). The maximal respiratory capacity (MRC) and the mitochondrial membrane potential ($\Delta\psi_m$) were also higher in cells treated with oxPAPC (Fig. 1a, c), pointing to increased activity of mitochondria and in the TCA cycle[21]. In contrast, 1,2-dipalmitoyl-*sn*-glycero-3-phosphocholine (DPPC) (an analog of PAPC that cannot be oxidized, and does not serve as a DAMP[7]) did not alter the metabolism of the cells (Supplementary Fig. 2a, b). Similar changes were also measured either in primary macrophages isolated from the peritoneal cavity or in granulocyte-macrophage colony stimulating factor (GM-CSF) bone marrow derived phagocytes that were exposed (or not) to LPS in the presence or absence of oxPAPC (Supplementary Fig. 1c-f).

Collectively, these findings indicate that the combined treatment of LPS and oxPAPC sustains a hypermetabolic state that is not supported by treatment with either PAMP or DAMP, individually.

Endogenous oxidized lipids promote the hyperproduction of IL-1β in LPS-stimulated macrophages.

Since production of IL-1β by macrophages is tightly regulated by metabolic changes[22, 23], we tested if the capacity of hypermetabolic cells to produce IL-1β is altered. oxPAPC did not induce IL-1β release by LPS-stimulated macrophages (Supplementary Fig. 2a and[6, 7]), but pro-IL-1β production was potently increased in cells exposed to different doses of LPS and oxPAPC, as compared to cells treated with LPS only (Fig. 2a, and Supplementary Fig. 2a). Secretion of TNF and IL-6 was unaltered or slightly increased, respectively (Fig. 2b, c and Supplementary Fig. 2b, c). In contrast, DPPC had no effect on cytokine production (Supplementary Fig. 2a-c). When cells were treated with ATP, to activate the NLRP3 inflammasome, the amount of IL-1β released was greater in LPS and oxPAPC co-treated cells than in cells treated with LPS only (Fig. 2d). Peritoneal macrophages also showed similar changes in cytokine production (Supplementary Fig. 2d-g). mRNA levels

demonstrated that this altered cytokine production was regulated transcriptionally (Fig. 2e). Finally, when we measured the production of pro-inflammatory cytokines in mice that were primed with LPS and subsequently challenged with oxPAPC, we recorded similar increases *in vivo* (Fig. 2f).

We next evaluated individual components present in the oxPAPC mixture for their capacity to boost IL-1β production and rewire cell metabolism, and found that PEIPC, but not the other moieties tested, recapitulated the behavior of oxPAPC (Supplementary Fig. 2h-l). Thus, while PGPC or POVPC induce the activation of the inflammasome (Supplementary Fig. 2h and[6]), PEIPC increases the expression of IL-1β. To test the hypothesis that individual components of oxPAPC independently potentiate the inflammatory activity of LPS, we administered a mixture composed of PEIPC and increasing doses of POVPC to macrophages that were primed with LPS. While concomitant administration of PEIPC and POVPC did not synergize to boost pro-IL-1β accumulation compared to cells treated with PEIPC only (Fig. 2g), secretion of IL-1β (but not of IL-6 or TNF) was significantly augmented in cells that were exposed to POVPC plus PEIPC (Fig. 2h-j).

Overall, this finding demonstrates that the individual moieties contained in oxPAPC work together to drive hyperinflammation by exerting non-redundant roles in macrophages. In support of this conclusion, we found that none of the metabolic changes induced by oxPAPC were dependent either on CD14 or TLR2 (Supplementary Fig. 2m-q), which instead recognize POVPC and PGPC to drive hyperctivation[6], or to potentiate the PPP and to favor ceramide accumulation[24], respectively.

Respiration maintenance promoted by oxPAPC enables LPS-stimulated macrophages to hyperproduce IL-1β.

To uncover a direct link between the maintenance of mitochondrial respiration, a characteristic of hypermetabolic cells, and the hyperinflammatory phenotype of macrophages co-exposed to LPS and oxPAPC, we inhibited respiration by targeting the complexes of the electron transport chain (ETC). Inhibition of the activity of each complex individually significantly decreased the capacity of hypermetabolic macrophages to produce IL-1β and to increase $\Delta\psi_m$ (Fig. 3a, b). In contrast, IL-1β production in cells exposed to LPS only was inhibited, as reported[25], when the activity of complex I or II (but not of complex III or IV) was disrupted (Fig. 3a). The functionality and expression of complexes I, II and IV were also increased in cells exposed to LPS and oxPAPC, compared to those treated with LPS only (Fig. 3c, and Supplementary Fig. 3a).

When cells are exposed to LPS, the production of nitric oxide (NO) blocks mitochondrial respiration, thus forcing glycolysis to sustain the production of ATP[18, 26]. When nitrite levels were measured, we found that oxPAPC administration to LPS-treated macrophages shuts down NO production in a dose-dependent manner, relative to its production in those treated with LPS only (Fig. 3d). This reduction was also associated with a significant decrease in *Nos2* gene transcription and iNOS protein (Fig. 3e, f). In agreement with our previous data, PEIPC (but not other components of oxPAPC) was found to play a similar role (Supplementary Fig. 3b). Addition of the NO donor S-Nitroso-N-acetyl-DL-penicillamine (SNAP) to macrophages exposed to LPS plus oxPAPC restored NO levels (Fig. 3g),

abrogated respiration (Fig. 3h), and down-modulated the expression of ETC complexes (Supplementary Fig. 3c); these changes were also accompanied by a significantly lower production of IL-1β (Fig. 3i). In addition, respiration and ETC complexes were maintained and IL-1β production was boosted in macrophages that were treated with LPS and also exposed to S-methyl iso-thiourea (SMIT, which inhibits NO production) (Fig. 3g-i), and Supplementary Fig. 3c). As reported[26], in *Nos2*$^{-/-}$ cells we found that IL-1β production was elevated in response to LPS, compared to that in wild type cells (Supplementary Fig. 3d). Notably, oxPAPC potently boosted IL-1β accumulation when added to *Nos2*$^{-/-}$ macrophages treated with LPS (Supplementary Fig. 3d), highlighting that oxPAPC also exert its hypermetabolic functions by additional means.

oxPAPC therefore protects LPS-treated macrophages from NO-dependent inhibition of mitochondrial respiration, and this process is necessary but not sufficient to induce the hyperinflammatory phenotype of cells exposed to LPS and oxPAPC.

Glutaminolysis is required to drive the hyperproduction of IL-1β in response to oxPAPC.

To ascertain if glucose utilization is necessary to drive the production of IL-1β in hypermetabolic cells, as it is in macrophages stimulated with LPS only, we used 2-DG or oxamate to block the first step or the last step of glycolysis, respectively. While oxamate abrogated IL-1β production in macrophages treated with LPS alone, it had no effect on the hyperproduction of IL-1β driven by oxPAPC (Supplementary Fig. 4a). 2-DG dampened IL-1β production under all the conditions tested (Supplementary Fig. 4a). Since 2-DG completely blocks glucose catabolism, we directly assessed the relevance of glucose abundance in the medium. While IL-1β production in macrophages treated with LPS was dependent on high glucose levels, when cells were treated with LPS and oxPAPC, IL-1β production was largely resistant to the reduction in glucose levels, to the point that cells cultured with no glucose were still able to produce a significant, although reduced, amount of IL-1β (Fig. 4a). Furhtermore, when pyruvate transport into the mitochondria was blocked, IL-1β production was only partially affected in macrophages exposed to LPS and oxPAPC, while, as reported[27], it was blocked in macrophages treated with LPS only (Supplementary Fig. 4a).

2-DG not only blocks glycolysis but also inhibits the TCA cycle[28]. We thus explored which substrates feed the TCA cycle of hypermetabolic macrophages to sustain IL-1β production. When fatty acid oxidation (FAO) was blocked, production of IL-1β by LPS-treated cells exposed, or not, to oxPAPC remained unaltered (Supplementary Fig. 4b). In contrast, glutamine deprivation, as well as the use of drugs that block glutamine metabolism, prevented the hyperproduction of IL-1β by macrophages treated with LPS and oxPAPC, without affecting, as previously reported[29], IL-1β production by macrophages treated with LPS only (Fig. 4b and Supplementary Fig. 4c). Dimethyl α-ketoglutarate (α-KG) (a cell-permeable form of α-KG, the end product of glutaminolysis) also restored IL-1β hyperproduction by cells treated with LPS and oxPAPC and cultured in the absence of glutamine (Fig 4c). When glucose was replaced with galactose, glutamine was sufficient to restore IL-1β production in cells treated with LPS and oxPAPC, but not in cells exposed to LPS only (Supplementary Fig. 4d). In the effort to assess if glutamine utilization could be

replaced by other substrates when cells are treated with oxPAPC, cells were cultured in media containing titrated levels of glutamine and/or glucose, and also added, or not, a lipid mix that can be utilized to produce energy: glutamine remained essential to drive the hyperproduction of IL-1β associated to exposure to LPS and oxPAPC (Supplementary Fig. 4e). Finally, we not only found that glutamine is essential to induce the hyperinflammatory phenotype in *Nos2*$^{-/-}$ cells exposed to LPS and oxPAPC (but not LPS only), but also that the boost in IL-1β production associated to iNOS-deficiency is completely lost when cells are exposed to oxPAPC in the absence of glutamine (Supplementary Fig. 4f).

Glutamine was strictly required also to sustain respiration and the MRC in cells treated with oxPAPC, in the presence or absence of LPS (Fig. 4d). We, thus, investigated the transcription levels of genes involved in glutamine metabolism and found that several major glutamine transporters, as well as other genes involved in glutamine metabolism, were significantly upregulated in cells exposed to oxPAPC only or LPS and oxPAPC (Fig. 4e, Supplementary Fig 4g). To investigate if glutamine utilization directly links mitochondria functionality to IL-1β production in cells exposed to oxPAPC, we performed a flow cytometric analysis in which we measured $\Delta\psi_m$ (to test mitochondrial activity) and the intracellular IL-1β content to correlate these two parameters at the single cell level. In the absence of glutamine, mitochondrial activity (in cells treated with LPS and oxPAPC or oxPAPC only) and IL-1β production (upon oxPAPC and LPS encounter) were profoundly affected (Fig. 4f, g). Low glucose levels altered instead the activity of macrophages treated with LPS only, leaving largely unaffected $\Delta\psi_m$ and IL-1β in cells exposed to oxPAPC (Fig. 4f, g).

Overall, these data demonstrate that oxPAPC administration rewires the metabolic needs of cells and boost IL-1β production by inducing a transcriptional program that, on the one hand, enables maintenance of mitochondrial respiration and, on the other hand, potentiates glutamine utilization.

Oxaloacetate accumulates in macrophages exposed to LPS and oxPAPC and potentiates IL-1β production.

Among the transcription factors that regulate IL-1β, HIF-1α is sensitive to metabolic alterations in the cell. Macrophages primed with LPS and then treated with oxPAPC expressed higher levels of HIF-1α, compared to those treated with LPS only (Fig. 5a, b), and enhanced HIF-1α expression was associated with increased transcriptional activity (Supplementary Fig. 5a, b) and IL-1β production (Fig. 5b). When HIF-1α was inhibited, IL-1β production was significantly decreased in LPS-treated cells that were exposed (or not) to oxPAPC (Supplementary Fig. 5c). When cells treated with LPS and oxPAPC were exposed to AA or to SNAP to inhibit mitochondrial respiration, the levels of HIF-1α, as well as that of IL-1β, were significantly decreased (Fig. 5c, d). We also observed a complete inhibition of HIF-1α (and IL-1β) accumulation when the cells were grown in a glutamine-free medium (Fig. 5e).

In LPS-stimulated macrophages, IDH is downregulated, allowing citrate accumulatation[18], and SDH is inhibited[22], driving reverse electron transport (RET), ROS production and stabilization of HIF-1α[25]. When we measured the levels of citrate, we found that it does not

accumulate in macrophages exposed to LPS and oxPAPC relative to those exposed to LPS only (Fig. 5f). Notably, glutamine (which is essential for driving the hypermetabolic and hyperinflammatory phenotype) makes a key contribution to the formation of citrate in cells treated with LPS and oxPAPC, compared to those treated with LPS only (Fig. 5g). We also found that IDHs were not downregulated and RET-dependent ROS production was not required to drive IL-1β production when cells were exposed to LPS and oxPAPC, compared to LPS only-treated cells (Supplementary Fig. 5d, e).

Since HIF-1α is tightly regulated by metabolites of the TCA cycle, such as succinate and itaconate[22, 30], we undertook a metabolomics analysis. oxPAPC treatment profoundly affected the metabolomics profile of macrophages stimulated, or not, with LPS (Fig. 5h and Supplementary Table 1). Succinate and itaconate were unchanged whether or not cells were treated with oxPAPC (Supplementary Fig. 5f, g). In agreement with these data, *Irg1* expression was unchanged in LPS-stimulated macrophages that were treated (or not) with oxPAPC (Supplementary Fig. 5h). In comparing the other metabolites of the TCA cycle in LPS-stimulated cells, we not only confirmed decreased citrate produciotn, but also found that oxaloacetate levels were dramatically increased in cells also treated with oxPAPC (Fig. 5i). In agreement with an earlier report *in silico* [31], the administration of oxaloacetate to macrophages stabilizes HIF-1α and, when cells are also exposed to LPS, potentiates IL-1β production (Fig. 5j, k).

Overall, these data demonstrate that oxPAPC treatment potentiates HIF-1α activity and IL-1β production by driving the accumulation of oxaloacetate in a process that occurs in the presence of an intact TCA cycle and independently of RET.

Citrate export to the cytoplasm, along with ACL activity, drive hyperinflammation in LPS-treated macrophages.

In macrophages treated with oxPAPC (either in the presence or absence of LPS) the ratio between citrate and oxaloacetate was changed in favor of this second metabolite (Fig. 5a). When we used ^{13}C-glutamine, we found that, in agreement with utilizing glutamine in the TCA cycle, oxaloacetate was enriched in M+2 and M+4, although other sources of carbon were also involved, as shown by an increase in M+0 (Supplementary Fig. 6a). In the TCA cycle, oxaloacetate is metabolized by citrate synthase (CS) or by malate dehydrogenase (MDH) 2 but we found no significant differences in the levels of CS mRNA or protein as well as *Mdh2* mRNA between cells treated or not with oxPAPC (Supplementary Fig. 6b-d). Oxaloacetate is also produced in the cytoplasm via: i) export of citrate through the citrate transport protein (CTP) into the cytoplasm, where it is metabolized by ACL into oxaloacetate; ii) malate conversion into oxaloacetate by the activity of MDH1. Although the transcriptional levels of CTP (*Slc25a1*) or *Mdh1* remained the same (Supplementary Fig. 6e, f), we found that the *Acly* transcript was significantly upregulated upon oxPAPC exposure (Fig. 6b). When we applied the mitochondrial CTP inhibitor (CTPi), or the ACL inhibitor BMS-303141 (ACLi), we found that IL-1β production and HIF-1α expression were significantly decreased in macrophages treated with LPS plus oxPAPC (Fig. 6c, d). Administration of a permeable form of citrate did not increase IL-1β production in cells treated with LPS only, suggesting that the transcriptional changes induced by oxPAPC (i.e.,

increased expression of *Acly*) are critical for driving the hyperinflammatory phenotype (Supplementary Fig. 6g). In contrast, CS inhibition significantly diminished IL-1β production in cells treated with LPS and oxPAPC (but not in macrophages activated by LPS only). Finally, our data show that administration of exogenous oxaloacetate bypassed the absence of glutamine as well as the inhibition of glutamine utilization, citrate transport into the cytoplasm, and citrate conversion into oxaloacetate (Fig. 6e).

Overall, our results support a model in which oxPAPC enables the formation of oxaloacetate, with export of citrate from mitochondria into the cytoplasm via CTP and citrate conversion via ACL playing fundamental roles. This process in turn potentiates HIF-1α expression and IL-1β production.

oxPAPC-driven immunometabolic adaptations occur in hypercholesterolemic mice.

Since IL-1β[32, 33] as well as exposure of macrophages to oxidized phospholipids[14, 34] make an essential contribution to the pathogenesis of atherosclerosis, we used hypercholesterolemic mice to explore whether the hyperinflammatory phenotype induced by oxPAPC is present in mice whose cells had been pre-exposed to oxidized phospholipids. A sublethal dose of LPS was administered *in vivo* to hypercholesterolemic *Ldlr*$^{-/-}$ or *Apoe*$^{-/-}$ mice exposed to a high fat diet, that present aortic root plaque formation (Supplementary Fig. 7a, b). Hypercholesterolemia led to a significant increase in the plasma levels of IL-1β and TNF (but not IL-6) five hours after LPS injection (Fig. 7a-c). Notably, this hyperinflammatory cytokine profile was also associated with an increased death rate in hypercholesterolemic mice relative to wild-type mice treated with LPS (Fig. 7d), while no significant differences were detected in mice fed a chow diet (Supplementary Fig. 7c). When glutamine utilization or ACL activity were inhibited, body temperature loss was prevented, IL-1β production was significantly decreased, and hypercholesterolemic mice were protected against death when injected LPS (Fig. 7e-g). These data led us to hypothesize that pre-exposure to oxidized phospholipids present in hypercholesterolemic mice can trigger the same hypermetabolic program that is induced by oxPAPC in cells primed with LPS. We found that cells exposed to oxPAPC for 24 hours showed increased $\Delta\psi_m$ compared to those left untreated, and that $\Delta\psi_m$ was further augmented early after LPS administration (Fig. 7h). Likewise, the MRC and basal glycolysis were significantly increased when cells were pre-exposed to oxPAPC (Fig. 7i). Similar results were obtained when the cells were pre-exposed to oxPAPC and analyzed 24 hours after LPS administration (Supplementary Fig. 7d). Both the protein and the mRNA levels for IL-1β and IL-6 were potently boosted, while levels for TNF were unaltered, and the production of NO (as well as the transcriptional levels of *Nos2*) was significantly reduced in cells treated with oxPAPC (but not with DPPC) for 24 hours and then activated with different doses of LPS (Fig. 7j, k and Supplementary Fig. 7e-i). Notably, cells incubated for 24 hours with oxPAPC, followed by LPS administration, assumed a hyperactive phenotype, as demonstrated by the release of IL-1β and the absence of cell death (Fig. 7j, Supplementary Fig. 7f, j). Finally, the increased production and release of IL-1β was abrogated when cells were cultured in a medium without glutamine, or following administration of GLSi, CTPi or ACLi (Fig. 7l).

Overall, these data demonstrate that, *in vitro* as well as *in vivo* in atherosclerotic mice, an encounter with oxPAPC drives the differentiation of hypermetabolic phagocytes that can mount a hyperinflammatory, lethal, response to LPS.

oxPAPC-driven immunometabolic adaptations can be targeted to decrease atherosclerosis.

Given that oxLDL aggregates that promote the development of atherosclerotic plaques have local concentrations of oxPAPC that can be as high as 100μM[35], we tested the capacity of oxLDL-driven foam cells (Supplementary Fig. 8a) to respond to LPS stimulation. Mitochondrial respiration was largely maintained and glycolysis was significantly increased in foam cells that were treated with LPS, relative to macrophages treated with LPS (Fig. 8a, b). Likewise, the $\Delta\psi_m$ was potently enhanced in foam cells relative to macrophages that were treated (or not) with LPS (Fig. 8c). Comparable increases in $\Delta\psi_m$ were also observed in peripheral blood monocytes of atherosclerotic mice (Supplementary Fig. 8b). Production of IL-6 and TNF was increased and NO was decreased in foam cells, relative to that in macrophages treated with LPS only, but IL-1β production was not boosted (Supplementary Fig. 8c-f). This is in agreement with reports[36, 37] that non-foamy cells, rather than foam cells, are the major contributors to IL-1β production in atherosclerotic plaques. In agreement with these data, oxPAPC administration does not induce accumulation of lipid droplets in the cells (Supplementary Fig. 8g) but when a high dose of a mix of lipids that induced a foamy phenotype (Supplementary Fig. 8h) was administered to cells treated (or not) with oxPAPC plus LPS, we found that IL-1β production was reduced (Supplementary Fig. 8i).

We, next, harnessed drugs that inhibit either glutamine utilization or oxaloacetate production, to decrease IL-1β levels in atherosclerotic mice. IL-1β in circulating monocytes of *Ldlr*$^{-/-}$ mice administered a high fat diet was significantly reduced upon blockade of glutamine usage or ACL inhibition (Supplementary Fig. 8j, k). When the aorta of atherosclerotic mice was analyzed, we found that IL-1β was produced exclusively by CD11b-positive cells and that, among these, CD64-positive macrophages were the major producers (Supplementary Fig. 8l). Based on this finding, we analyzed the production of IL-1β in macrophages resident in the plaque and found that GLSi or ACLi significantly decreased IL-1β accumulation (Fig. 8d, e). In agreement with the essential role of IL-1β during atherosclerosis, these treatments significantly decreased the size of the atherosclerotic plaques, relative to that in mice not treated with the inhibitors (Fig. 8f). The levels of cholesterol were not affected by drug treatments (Supplementary Fig. 8m), excluding a generic alteration in body metabolism.

Finally, we determined if oxPAPC alters the gene expression of key metabolic regulators in a human population by analyzing the peripheral blood transcriptional signature from 4,052 participants of the Framingham Heart Study (FHS) Offspring and Third Generation cohorts[38]. Specifically, we tested the association between transcriptome-wide gene expression and circulating Total Cholesterol (TC), LDL-cholesterol (LDL-C), HDL-cholesterol (HDL-C) and triglycerides (TG) (Supplementary Table 2). Then, we created a consolidated averaged gene-ranking of a pro-atherosclerotic lipid profile (higher TC, LDL-C, TG, and lower HDL-C) and performed Gene Set Enrichment Analysis (GSEA) to

determine if the cluster of genes upregulated by oxPAPC in mice are also differentially expressed in humans with the pro-atherosclerotic lipid profile (Fig. 8g). Consistent with our expectation, we found that the mouse oxPAPC signature was also enriched in FHS participants with a pro-atherosclerotic lipid profile (Fig. 8h). Furthermore, we found that the signature of glutamine utilization, citrate and oxaloacetate metabolism as well as mitochondrial respiration were also significantly enriched in relation to the pro-atherosclerotic lipid profile (Supplementary Fig. 8n). Fatty acid utilization was also found to be enriched, as expected in patients that have abnormal circulating lipid levels (Supplementary Fig. 8n). On the contrary, the glucose utilization signature, as well as the leukocyte migration one (that was used as a negative control) were not significantly enriched in our analysis (Supplementary Fig. 8n).

Together, these results demonstrate that in atherosclerotic mice and hypercholesterolemic humans, an encounter with oxPAPC drives the differentiation of hypermetabolic phagocytes with a hyperinflammatory phenotype (Extended Data Fig. 1).

DISCUSSION

Metabolic changes that occur during inflammation determine macrophage fate and the potency of the immune response. Here we document that oxPAPC induces a hypermetabolic state within macrophages. In particular, in mice and humans, oxPAPC controls gene transcription to favor the mitochondrial respiration, glutamine catabolism, and oxaloacetate accumulation that globally drive IL-1β accumulation. Also, that the hypermetabolic state induced by oxPAPC can be targeted to reduce inflammation upon LPS encounter or to protect against atherosclerosis development.

We demonstrated that individual components contained in oxPAPC make specific contributions to the induction of hyperinflammation: while POVPC and PGPC drive inflammasome activation[6, 7], PEIPC regulates the hypermetabolic state characterized by IL-1β accumulation. When cells are pre-exposed to oxPAPC, they become both hyperactive and hypermetabolic, and the mRNA for IL-1β is rapidly upregulated after LPS administration, compared to cells that are first primed with LPS and then treated with oxPAPC. A possible explanation for this is that the moieties that allow inflammasome activation, and also the metabolites (i.e.: oxaloacetate) that characterize the hypermetabolic phenotype, have time to accumulate in cells that are pre-incubated with oxPAPC, and thus they can immediately exert their activity. These results further highlight the complexity of the action of oxidized phospholipids, which function in a context-dependent manner.

Our findings also highlight the striking metabolic similarity between hyperinflammatory macrophages exposed to oxPAPC and LPS and classical M2 macrophages, which also rely on glutaminolysis and respiration to exert their functions[16, 28]. How cells at the opposite spectrum of the inflammatory response share such a high metabolic homology remains a puzzle, though we speculate that the genetic and epigenetic changes regulated either by the $\Delta\psi_m$[39] or by glutamine metabolism (as shown in T cells[40]) differentially affect the responses of the two cell types.

When citrate is exported to the cytoplasm in macrophages treated with LPS only, oxaloacetate does not accumulate; instead, it is converted into aspartate in LPS-treated cells and is used in two ways: i) in the aspartate-arginosuccinate shunt to replenish the broken TCA cycle[18]; and ii) to produce arginine, which is in turn utilized by iNOS to produce NO and citrulline. Our metabolomic analysis demonstrated that levels of aspartate and citrulline were decreased in cells treated with oxPAPC and LPS, compared to those treated with LPS only, in agreement with our findings that the TCA cycle is not broken and that NO production is reduced following oxPAPC treatment. These data link the decrease in NO production with the accumulation of oxaloacetate in macrophages exposed to LPS and oxPAPC.

Our results are relevant in the context of atherosclerosis. Monocytes and macrophages derived from patients with arterial diseases reveal an increased inflammatory phenotype associated with the elevated production of IL-6 and IL-1β[41], each of which is a cytokine that is also potently induced by oxPAPC-treated cells. Our findings also show that macrophages associated with the development of atherosclerosis exhibit the classical metabolic features of oxPAPC-treated phagocytes. Upon oxPAPC administration, glutamine utilization is favored by the upregulation of several glutamine transporters, an event that happens independently of the presence or absence of LPS. This process poises oxPAPC-exposed cells to switch to the new metabolic state and may explain why cells pre-exposed to oxPAPC. Notably, in atherosclerotic lesions, glutamine accumulates and is preferentially used (over glucose) by macrophages as an energy substrate[42]. Nevertheless, macrophages are not the only target of oxPAPC. Our data on GM-CSF-derived phagocytes as well as data in the literature on endothelial cells[43] demonstrate that oxPAPC-dependent metabolic changes are not unique to macrophages or even immune cells. It will be important in future studies to address the moieties contained in oxPAPC that alter the metabolism of other cell types and how these changes affect inflammation and/or atherosclerosis.

Our observations also complement recent reports that prolonged exposure to oxLDL induces epigenetic changes, which then drive the formation of trained phagocytes[44]. Of note, IL-1β drives the long term training of monocyte precursors[45], leading us to postulate the existence of a time window wherein oxPAPC-driven immunometabolic changes drive augmented IL-1β production, which in turn supports the differentiation of trained pro-inflammatory precursors.

Finally, low levels of LPS are strong drivers of atherosclerosis[46], as is TLR4[47]; and subclinical endotoxemia is also a possible risk factor for atherosclerosis in humans[48]. Based on these reports, we conclude that the inflammatory effect of LPS during atherosclerosis development is amplified by oxidized phospholipids present in the blood of atherosclerotic patients[49]. Earlier reports have concluded that CD14 is not involved in atherosclerosis in mice[50], highlighting the contribution of CD14-independent immunometabolic activities elicited by LPS and oxidized phospholipids to the development of atherosclerosis.

In conclusion, our findings that pharmacological inhibitors of glutamine utilization or oxaloacetate formation can protect against LPS-induced hyperinflammation, and at the same

time reduce atherosclerotic plaque formation, strongly suggest that these approaches can be used to develop novel therapeutics to intervene against the development of atherosclerosis.

METHODS

Mouse strains and cell culture.

C57BL/6J (Jax 000664), *Cd14*$^{-/-}$ (Jax 003726), *Nos2*$^{-/-}$ (Jax 002609), *Tlr2*$^{-/-}$ (Jax 004650), *Apoe*$^{-/-}$ (Jax 002052), and *Ldlr*$^{-/-}$ (Jax 002207) and mice were purchased from Jackson Labs. Phagocytes were differentiated from bone marrow in DMEM (Gibco), 30% L929-M-CSF (macrophages, BMDMs) or 10% B16-GM-CSF supernatant, and 10% FBS. Foam cells were derived by incubating bone marrow macrophages with oxLDL (200 μg/ml) for 4–24 hours before stimulation. Primary peritoneal macrophages were obtained from peritoneal lavage of mice i.p. treated with 4% thioglycollate for 4 days. Prior to stimulations, cultured cells were PBS washed and re-plated in DMEM supplemented with 10% FBS at a concentration of 1×10^6 cells/ml. In substrate restriction experiments, macrophages were stimulated in DMEM (without glucose, glutamine and pyruvate, Thermo) supplemented with 10% dialyzed FBS (Thermo) and with the indicated concentrations of glucose and/or glutamine (Thermo). In all the experiments that required LPS priming, LPS was used at 1μg/ml for 3h unless otherwise specified.

Antibodies and reagents.

E. coli LPS (Serotype O555:B5-TLRgrade™) was purchased from Enzo. oxPAPC was purchased from Avanti Polar Lipids or custom made. DPPC, PAPC, PGPC, POVPC, LysoPC were purchased from Avanti Polar Lipids. KOdiAPC was purchased from Cayman Chemicals. oxLDL were purchased from Alfa Aesar. ATP, oligomycin, FCCP, rotenone, antimycin A, sodium azide, TMPD, ascorbate, pyruvate, malate, succinate, dimethyl malonate, dimethyl α-ketoglutarate, triethyl citrate, succinyl-CoA, SNAP, SMIT, 2-DG, oxamate, UK5099, CB-839, BPTES, EGCG, etomoxir, mildronate, trimetazidine, CTPi, BMS-303141 (ACLi), oxaloacetate, Oil Red O and hematoxylin were purchased from Sigma. Glutamine and lipid mix (chemically defined lipid concentrate) were purchased from Thermo. MitoQ and CAY-10585 were purchased from Cayman Chemicals.

The following antibodies were used for immunoblotting: OXPHOS Cocktail (1:250, ab110413, Lot# K2342, Abcam), HIF-1α (1:500, NB100–449, Lot# A6, Novus Biologicals), iNOS (1:500, PA1–036, Lot# QD213201, Thermo Fisher Scientific), IL-1β (1:1000, AF-401-NA, R&D Systems), CS (1:1000, 14309, Lot#1, Cell Signaling Technology), HSP60 (1:500, 681502, P83G8 clone, Lot# B206372, BioLegend), β-Actin (1:3000, A5441, AC-15 clone, Lot# 127M4866V, Sigma). The following antibody were used for IHC: CD68 (1:500, 137002, FA-11 clone, BioLegend), IL-1β (1:300, ab9722, Abcam). For fluorescence-based assays, the fluorophore-conjugated antibodies and reagents were used as the following: Zombie violet (BioLegend), Sytox Blue (BioLegend), APC Annexin V (BioLegend), TMRM (Thermo), MitoTracker Green (Thermo), MitoTracker Deep Red (Thermo), PE Pro-IL-1β (1:500, 12–7114-82, NJTEN3 clone, Lot#1992335, Thermo Fisher Scientific), Tom20 (1:250, sc-11415, FL-145, Lot# C1416, Santa Cruz Biotechnology), Alexa488 Anti-rabbit (1:250, A21441, Lot# 1697089, Thermo Fisher Scientific), APC

HIF-1α (1:50, IC1935A, Lot# AAMC0218051, R&D Systems), BV510 CD45 (1:200, 103138, 30-F11 clone, BioLegend), FITC CD11b (1:200, 101206, M1/70 clone, BioLegend), APC/Cy7 CD11b (1:200, 101226, M1/70 clone, BioLegend), BV711 CD64 (1:200, 139311, X54–5/7.1 clone, BioLegend), APC Ly6G (1:200, 127614, 1A8 clone, BioLegend), PerCP/Cy5.5 Ly6C (1:200, 128012, HK1.4 clone, BioLegend), Pacific Blue I-A/I-E (1:200, 107620, M5/114.15.2, BioLegend).

Lipid oxidation.

PAPC was oxidized using a method similar to previously reported[51]. Briefly, PAPC (Avanti Lipids) was transferred to clean borosilicate tubes in 0.5–1 mg aliquots in chloroform, dried, and oxidized for 24–72 hours, while monitoring oxidation by flow injection on an ESI instrument (Thermo LCQ). Lipid was oxidized to maximize level of PEIPC and analyzed by phosphorus assay for concentration.

PEIPC Purification.

PEIPC was separated from other components using a method similar to previously reported[51]. Briefly, normal phase high performance liquid chromatography (NP-HPLC) was performed by loading oxPAPC resuspended in methanol onto a silica column and eluting isocratically with a mobile phase of 77:8:15 acetonitrile:methanol:water at a flow rate of 2 ml/min. Reverse phase HPLC (RP-HPLC) was performed by loading samples resuspended in methanol onto a C8 column (250×5mm) and eluting with a methanol-water mobile phase, starting at 50:50 methanol:water up to 100% methanol. One notable difference in recent methods is that oxPAPC is preseparated using C8 SPE columns (Phenomenex) to avoid degradation of LC-MS columns. HPLC fractions were continuously monitored by ESI-MS and fractions of interest were collected. SPE samples were also analyzed by flow injection ESI-MS. In order to best separate PEIPC from other oxPAPC, SPE, NP-HPLC, and RP-HPLC all needed to be used on samples.

Mitochondrial potential and viability measurements by flow cytometry.

Cells were treated as indicated and then co-stained with TMRM (100 nM) and MitoTracker Green (20 nM) for 15 min at 37°C. Cells were washed, resuspended in PBS containing Annexin-V and Sytox Blue for 15 min and then analyzed by flow cytometry. $\Delta\psi_m$ was calculated using FlowJo (FlowJo LLC) as the derived parameter on the ratio between TMRM and MitoTracker Green signals. The same strategy was used also when MitoTracker Deep Red (20 nM) and anti-TOM20 were used for $\Delta\psi_m$ quantification in fixed cells.

Seahorse metabolic analysis

Oxygen consumption rate (OCR) and extracellular acidification rate (ECAR) were measured with a Seahorse XFe96 Extracellular Flux Analyzer.

Macrophages (5×10^4 per well) were seed in a seahorse 96-well plate in DMEM supplemented with 10% FBS and treated as indicated. After 24 hours, cells were washed twice and incubated in the Seahorse Assay Medium supplemented with 25 mM glucose and 2 mM glutamine at 37°C for 45 min. The OCR and ECAR were measured under basal conditions and after injection of OM (1.5 μM), FCCP (1.5 μM) plus pyruvate (10 mM),

rotenone (0.5 μM) plus antimycin A (0.5 μM) (Rot.+AA), and 2-DG (50 mM). Metabolic parameters were calculated as follows: Basal OCR = $OCR_{before\ OM}$ - $OCR_{after\ Rot+AA}$, ATP-linked respiration = Basal OCR - $OCR_{after\ OM}$, Maximal Respiratory Capacity (MRC) =$OCR_{after\ FCCP+Pyruvate}$ - $OCR_{after\ Rot+AA}$, Basal ECAR = $ECAR_{before\ OM}$ - $ECAR_{after\ 2\text{-}DG}$, Maximal Glycolytic Capacity (MGC) = $ECAR_{afterOM}$ - $ECAR_{after\ 2\text{-}DG}$.

For electron flow activity experiments, macrophages were seeded as described above and treated as indicated. After 24h cells were washed and incubated in mannitol and sucrose (MAS) medium containing plasma membrane permeabilizer (XF PMP 1 nM), FCCP (4 μM) and pyruvate/malate (10 mM/0.5 mM, specific substrate for complex I). In order to visualize the activity of different mitochondrial respiratory complexes, OCR was analyzed during basal conditions (complex I activity) and injecting rotenone (2 μM) (to block complex I), succinate (10 mM) (to induce complex II activation), AA (2 μM) (to block complex III) and TMPD (200 μM) plus ascorbate (10 mM) (to induce complex IV activation). Each complex activity was calculated as follows: Complex I= $OCR_{before\ Rot.}$ - $OCR_{after\ Rot}$, Complex II = $OCR_{after\ succinate}$ − $OCR_{after\ AA}$, Complex IV = $OCR_{after\ TMPD/ascorbate}$.

For glutamine metabolism experiments, macrophages were seeded as described above and treated as indicated. After 24h cells were washed and incubated in in the Seahorse Assay Medium supplemented with 25 mM glucose only at 37°C for 45 min. The OCR was measured under basal conditions and after injection of glutamine (2mM), OM (1.5 μM), FCCP (1.5 μM) and rotenone (0.5 μM) plus antimycin A (0.5 μM) (Rot.+AA).

Upon completion of each Seahorse assay, DNA content was measured by fluorescence (CyQUANT, Thermo) to normalize ECAR and OCR to the number of cells.

Gene expression analysis and ELISA.

RNA was isolated from cell cultures using GeneJET RNA Purification Kit (Thermo). Purified RNA was analyzed for gene expression on a CFX384 real time cycler (Bio-rad) using TaqMan RNA-to-CT 1-Step Kit (Thermo) with probes purchased from Thermo specific for *Il6* (Mm00446190_m1), *Tnf* (Mm00443258_m1), *Il1b* (Mm00434228_m1), *Nos2* (Mm00440502_m1), *Egln3* (Mm00472200_m1), *Glut-1* (Mm00441480_m1), *Pgd* (Mm00503037_m1), *G6pdx* (Mm00656735_g1), *Idh1* (Mm00516030_m1), Idh2 (Mm00612429_m1), *Idh3a* (Mm00499674_m1), *Idh3b* (Mm00504589_m1), *Idh3g* (Mm00599689_m1), *Irg1* (Mm01224532_m1), *Acly* (Mm01302282_m1), *Cs* (Mm00466043_m1), *Mdh1* (Mm00485106_m1), Mdh2 (Mm00725890_s1) and *Slc25a1* (Mm00467666_m1). For expression analysis of glutamine-related genes, iTaq Universal SYBR Green One-Step Kit (Bio-rad) was used in association with specific KiCqStart SYBR Green Primers (Sigma) for the following genes: *Slc1a5*, *Slc3a2*, *Slc7a5*, *Slc38a1*, *Slc38a2*, *Gls*, *Gls2*, *Glud1*, *Got1*, *Got2*, *Gpt*, *Gpt2*, *Nadsyn1*, *Gfpt1*, *Gfpt2*, *Gmps*, *Ppat*, *Asns* and *Cad*. ELISA for IL-6, IL-1β and TNF were performed using Mouse Ready-SET-Go ELISA kits (eBioscience).

Nitrite quantification.

Cell culture supernatants were collected after each experiment and stored at −20°C prior analysis.

Nitrite concentrations were measured using Greiss reagent (Sigma) according to manufacturer instructions.

Immunoblotting.

For Western blotting, bone-marrow derived macrophages (1×10^6) were stimulated with ligands for indicated periods, and subsequently lysed in 100 μl of RIPA buffer. Protease inhibitors and phosphatase inhibitors (Thermo) were added just prior to cell lysis. Immunoblotting was performed using standard molecular biology techniques.

Multiparameter Intracellular Staining.

Macrophages were stimulated as described and incubated for 15 min in PBS containing Zombie violet dye and/ or MitoTracker Deep Red. Cells were washed, fixed with the Fixation Buffer (BioLegend) and permeabilized with the Intracellular staining permeabilization buffer (BioLegend). Mitochondrial mass was analyzed using the TOM20 antibody and the anti-rabbit Alexa488. HIF-1α and pro-IL-1β content were analyzed using APC anti-HIF-1α (R&D) and PE anti-pro-IL-1β (NJTEN3 clone, Thermo). Dead cells (Zombie violet dye positive cells) were excluded from following analysis.

Metabolomic analysis.

Metabolomics profiling and ^{13}C metabolic flux analysis were performed at the Beth Israel Deaconess Medical Center Mass Spectrometry Facility. Briefly, polar metabolites were collected by methanol-based extraction as previously described[52]. Samples were re-suspended using HPLC grade water for mass spectrometry and analyzed using a 5500 QTRAP hybrid triple quadrupole mass spectrometer (AB/SCIEX) coupled to a Prominence UFLC HPLC system [52]. A total of 284 endogenous water-soluble metabolites were analyzed. For ^{13}C metabolic flux analysis, macrophages were incubated for at least 4h with DMEM (without glucose, glutamine and pyruvate, Thermo) supplemented with 10% dialyzed FBS (Thermo), glucose (25 mM, Thermo) and [U-^{13}C]-glutamine (2mM, Cambridge Isotope Laboratories). Polar metabolites were extracted as described above and analyzed as previously described[53]. Statistical analysis was performed using MetaboAnalyst (http://www.metaboanalyst.ca, free online software).

Oxaloacetate and citrate quantification.

Macrophages (2×10^6) were stimulated as described and homogenized. Cell lysates were deproteinized using 10 kDa molecular weight cut off spin columns (BioVision) and analyzed using oxaloacetate or citrate fluorescent kits (BioVision). The concentrations of metabolites were normalized for the protein content, using the BCA assay (Thermo) before the deproteinizing step.

ORO staining of fixed cells.

Cells treated as indicated or aorta sections were fixed with 10% formalin for 30 min, washed and incubate with isopropanol 60% for 5 min. Samples were stained with ORO (2mg/ml, 5 min) and hematoxylin (1 min).

In *vivo* oxPAPC challenge.

Female mice aged 8 weeks were primed via intraperitoneal (i.p.) injection with 1 mg/Kg *E. coli* LPS or vehicle control for 5 hours. Mice were then challenged via i.p. injection of oxPAPC (80mg/Kg) or control vehicle. Serum blood samples were collected 4 hours post-priming and 2 hours post-challenge for cytokine analysis. All animal procedures were approved by IACUC.

Hypercholesterolemic mice.

WT, *Apoe*$^{-/-}$ and *Ldlr*$^{-/-}$ 8-week old female mice were feed for 4 weeks with a high-fat diet (TD.88137 Envigo) and then treated i.p. with 1mg/Kg *E. coli* LPS. Where indicated mice were treated with GLSi (CB-839, 12.5 mg/Kg, i.p.) or ACLi (BMS-303142, 10 mg/Kg, oral gavage). Blood was collected after 5 hours and the indicated cytokines were analyzed by ELISA. Body temperature was measured after 8h with a rectal probe. Mice survival was monitored for 30/40h after LPS injection. To analyze lesions in the aortic root, mice were anesthetized, euthanized and hearts were perfused with PBS and incubated in 4% PFA overnight. After incubation in 15–30% sucrose and OCT inclusion, serial cryosections of 10 μm thickness were taken from the region of the proximal aorta through the aortic sinuses and stained with ORO/hematoxylin or Masson's Tricrome stainig (MTS). Aorta cryosections were also incubated with rabbit anti-IL-1β (Abcam) and rat anti-CD68 (BioLeged, FA-11 clone) and fluorescently stained with anti-rabbit-Cy3, anti-rat-AlexaFluor647 and DAPI. Images were acquired with a Leica LSM 880 confocal laser scanning microscope. For blood collection, mice were fasted for 12 hours before retro-orbital bleeding. Plasma was separated by centrifugation and total blood cholesterol was quantified with the Amplex red cholesterol assay kit (Molecular Probes). Alternatively, blood was collected from the indicated mice and analyzed by flow cytometry for mitochondrial potential (TMRM) in cells positive for the staining with the anti-CD11b^{+} and anti-IA/IE^{+} antibodies or for pro-IL-1β production in monocytes (CD11b^{+}Ly6G^{-}Ly6C^{+} cells). For the analysis of aorta-associated cells, mice were perfused with cold PBS plus heparin (10U/ml) and whole aorta was isolated and incubated in an enzymatic digestion buffer (400 U/ml collagenase type I, 120 U/ml collagenase type XI, 60 U/ml hyaluronidase and 60 U/ml DNase I, 20 mM HEPES in HBSS containing calcium) for 50 min at 37 °C. The resulting cell suspension was filtered and washed with cold PBS before proceeding to the staining protocol for the indicated surface markers and for intracellular pro-IL-1β.

Statistical analysis.

Statistical significance for experiments with more than two groups and two factors was tested with two-way ANOVA, and Sidak's, Dunnet's or Tukey's multiple-comparison tests were performed according to the nature of the comparison tested. One-way ANOVA with Turkey's multiple-comparison test was used to analyze statistically significant differences between the means of two or more independent groups. To establish the appropriate test, normal distribution and variance similarity were assessed with the D'Agostino-Pearson omnibus normality test using Prism8 (Graphpad) software. When comparisons between only two groups were made, an unpaired two tailed *t*-test was used to assess statistical significance. For survival experiments, *P* values were determined by long-rank test and

adjusted with Bonferroni correction. Adjusted *P* values were calculated with Prism8 (Graphpad). Asterisks were used as follows (also indicated in figure legends): **P* < 0.05, ***P* < 0.01, ****P* < 0.001 and *****P* < 0.0001. The exact values for both significant and non-significant P values as well as the statistical analysis used are available in in the "Supplementary Information", SOURCE DATA section.

Framingham Heart Study cohort analyses.

Gene expression and lipid profiling were available for 5,626 participants from the Offspring and Third Generation cohorts of the FHS. Recruitment procedures and clinical assessments of these cohorts have been previously described[54]. Samples for the current analyses were obtained from Offspring cohort participants that attended the eighth examination cycle (2005–2008) and Third Generation cohort participants that attended the second examination cycle (2008–2011). We excluded individuals from analyses that were taking lipid-lowering medications (n=1,574), leaving 4,052 participants in the study sample (mean age 52.0 [standard deviation 12.8] years, 58% female). The FHS was approved by the Boston University Medical Center Institutional Review Board, and all the participants provided written informed consent.

Peripheral blood samples were collected in the morning from participants after an eight-hour fast. Total cholesterol (TC), high-density lipoprotein cholesterol (HDL-C) and triglycerides (TG) were measured via an enzymatic colorimetric assay (Roche Hitachi 911, Roche Diagnostics) and low-density lipoprotein cholesterol (LDL-C) was calculated by the Friedewald equation. The mean sample TC was 193 (SD 34) mg/dL, HDL-C 61 (18) mg/dL, LDL-C 110 (30) mg/dL, and TG 109 (69) mg/dL. The processing of samples for gene expression profiling has been previously described[55]. Briefly, total RNA was isolated from whole blood using PAXgene blood tubes (PreAnalytiX, Hombrechtikon, Switzerland) and amplified using the WT-Ovation Pico RNA Amplification System (NuGEN, San Carlos, CA). The obtained cDNA was hybridized to the Affymetrix Human Exon 1.0 ST Array (Affymetrix, Inc., Santa Clara, CA). Signal intensities from the image scanner were then quantile-normalized and log2 transformed, followed by summarization using Robust Multi-array Average[56]. The annotation for each transcript was obtained from Affymetrix NetAffx Analysis Center (version 31).

Linear mixed effects models were used to test associations between TC, LDL-C, HDL-C, and TG with gene expression, adjusted for age, sex, body mass index, imputed cell counts[57], and technical covariates as fixed effects, and family relatedness as a random effect. Analyses were performed using the *pedigreemm* R package (www.r-project.org/). A conservative Bonferroni correction ($p < 0.05$ / number of transcripts tested) was used to account for multiple testing.

Next, we performed pathway analysis using Gene Set Enrichment Analysis (GSEA) with the fgsea R package. While gene expression can be correlated with all four lipid parameters (TC, LDL-C, HDL-C, and TG), this strategy would lead to four distinct pathway analyses, which would require a complex interpretation. To enhance insight, we instead aimed at consolidating information coming from the four lipids into a single metric. Given that GSEA requires gene rankings, we utilized a consolidated gene ranking approach. First, we sorted

genes by signed p-values (with sign from the linear model coefficient), such that genes with small p-values for positive coefficients are placed at the top of the ranking. Whenever more than one probeset was available for a gene (4.9% of linear model coefficients), the most statistically significant probeset (without regards to the direction of change) was selected. We plotted rankings against each other (Supplementary Fig. 8o) and noticed that HDL-C driven rankings were generally inversely correlated with rankings driven by TC, LDL-C, and TG, in line with the well-known inverse relationship between HDL-C and triglycerides and positive correlation of TC and LDL-C. Therefore, we averaged the four rankings (for HDL, the reversed ranking was used), yielding a single averaged pro-atherosclerotic lipid profile ranking (higher TC, LDL-C, TG, and lower HDL-C) for GSEA analysis. To validate the mouse findings, we conducted enrichment testing for the principal energy pathways that feed the TCA cycle (from GO databases or custom gene sets that integrate/expand existing gene lists). The tested pathways included:

a)Gene sets derived from Gene Ontology (GO) collection:

Fatty acid beta oxidation (GO:0006635), Cellular respiration (GO:0045333), Glucose metabolic process (GO:0006006) and Leukocytes migration involved in inflammatory response (GO:0002523)

b)Manually curated gene sets:

oxPAPC Signature: *Il1b*, *Slc3a2*, *Egln3*, *Acly*, *Nadsyn1*, *Cad*, *Slc5a1*, *Got1*, *Asns*, *Idh3a*, *Slc7a5*, *Idh1*, *Slc2a1*, *Idh2*, *Il6*, *Idh3g*.

Citrate/OAA: *Slc25A1, Pck1, Pck2, Pcx, Mdh1, Mdh2, Got1, Got2, Cs, Irg1, Aco1,Aco2, Acly*.

Glutamine: *Aadat, Abat, Acy3, Adsl, Adss, Adssl1, Agmat, Agxt, Agxt2, Aldh18a1, Aldh4a1, Aldh5a1, Amdhd1, Arg1, Arg2, Art4, Asl, Asns, Asnsd1, Aspa, Asrgl1, Ass1, Cad, Cps1, Ctps, Ctps2, Dao, Ddah1, Ddah2, Ddo, Fah, Fpgs, Ftcd, Gad1, Gad2, Gclc, Gclm, Gfpt1, Gfpt2, Ggh, Ggt1, Gls, Gls2, Glud1, Glud2, Glul, Gmps, Got1, Got2, Gpt, Gpt2, Hal, Il4i1, Lgsn, Mecp2, Mthfs, Nags, Nit2, Nos1, Nos2, Nos3, Noxred1, Oat, Otc, Pfas, Phgdh, Ppat, Prodh, Prodh2, Pycr1, Pycr2, Pycrl, Sirt4, Slc1a3, Tat, Uroc1, Slc1a5, Slc6a1, Slc6a19, Slc7a5, Slc7a6, Slc7a7, Slc7a8, Slc7a9, Slc38a1, Slc38a2, Slc38a3, Slc38a5, Slc38a7, Slc38a8*.

In the heatmap, regression coefficients from linear modeling were first standardized (but not centered, to preserve directionality) before plotting to allow comparability on the same scale across TC, LDL-C, HDL-C, and TG. *Nos2* is shown in the heatmap but not in the GSEA because, contrary to the other genes, it is downregulated instead of upregulated in mouse cells treated with oxPAPC.

Data availability.

The data that support the findings of this study are available from the corresponding author upon request. The “Life Science Reporting Summary” is available on-line. Uncropped raw

immunoblot images can be found in the “Supplementary Information”, SOURCE DATA section.

Participant-level phenotype and genotype data from the Framingham Heart Study are accessible from the U.S. National Center for Biotechnology Information (NCBI) database of Genotypes and Phenotypes (dbGaP) at https://dbgap.ncbi.nlm.nih.gov/ to approved scientific investigators pursuing research questions that are consistent with the informed consent agreements provided by individual research participants. The FHS expression data are available at dbGaP at the following URL:https://www.ncbi.nlm.nih.gov/projects/gap/cgi-bin/study.cgi?study_id=phs000363.v3.p6.

Extended Data

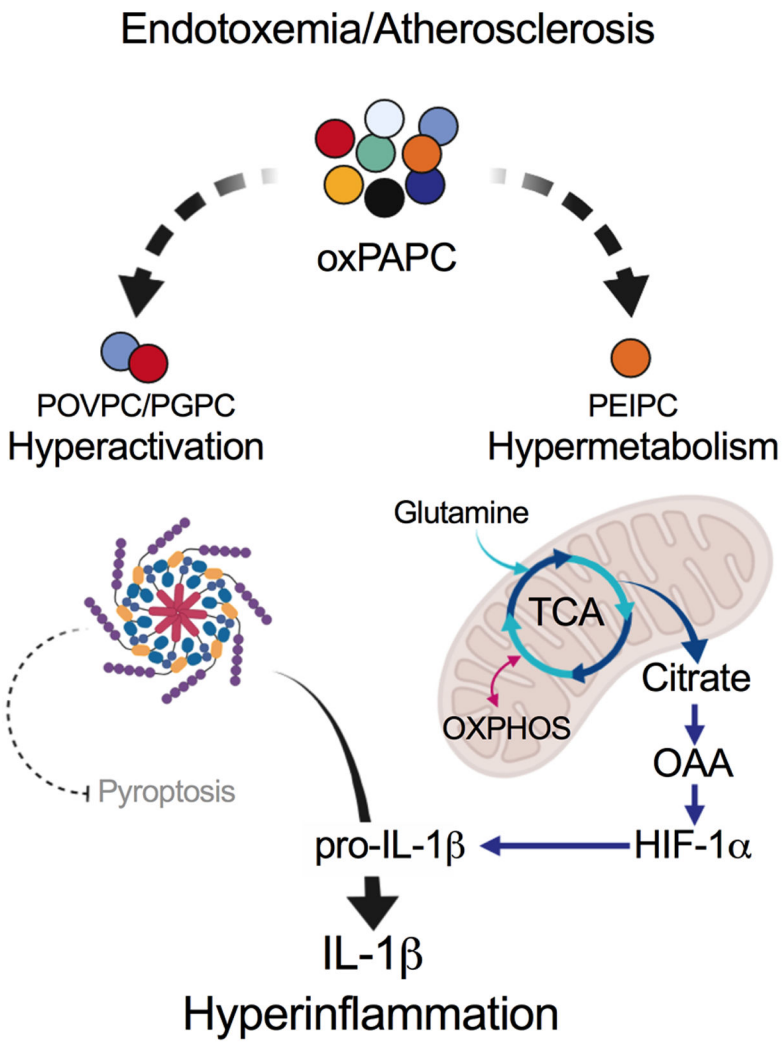

Extended Data Fig. 1. oxPAPC drives hyperactivation and hypermetabolism in macrophages.
Schematic depicting oxPAPC activities. oxPAPC is a mixture of oxidized phospholipids that induce an hyperinflammatory state in phagocytes upon LPS encounter and/or during atherosclerosis development. Moieties such as POVPC or PGPC contained in oxPAPC drive the formation of hyperactive cells that are characterized by inflammasome activation in the absence of pyroptosis. In contrast to POVPC or PGPC, PEIPC engages a hypermetabolic state in phagocytes that favors IL-1β accumulation and that is characterized by: i) the simultaneous activation of OXPHOS and aerobic glycolysis; ii) glutamine utilization to feed the TCA cycle; iii) oxaloacetate (OAA) accumulation in the cytoplasm to potentiate HIF-1α activation.

Supplementary Material

Refer to Web version on PubMed Central for supplementary material.

ACKNOWLEDGMENTS

We thank Drs. F. Granucci, J. C. Kagan and L. R. Marek for discussion, help and support. RS thanks the UCLA QCBio Collaboratory community directed by Dr. M. Pellegrini.

IZ is supported by NIH grant 1R01AI121066, 1R01DK115217, and NIAID-DAIT-NIHAI201700100. JRS is supported by NIH grant 1R15HL121770-01A1.

The Framingham Heart Study is funded by National Institutes of Health contract N01-HC-25195 and HHSN2682015000001I. The laboratory work for the FHS investigation was funded by the Division of Intramural Research, National Heart, Lung, and Blood Institute, National Institutes of Health, and by a Director's Challenge Award, National Institutes of Health (DL, PI). This study utilized the computational resources of the Biowulf system at the National Institutes of Health, Bethesda, MD (http://biowulf.nih.gov). MMM is supported by the NIH grant K99HL136875. The content is solely the responsibility of the authors and does not necessarily represent the official views of the National Institutes of Health.

REFERENCES

1. Brubaker SW, Bonham KS, Zanoni I & Kagan JC Innate Immune Pattern Recognition: A Cell Biological Perspective. Annu Rev Immunol (2015).
2. Janeway CA Jr. Approaching the asymptote? Evolution and revolution in immunology. Cold Spring Harb Symp Quant Biol 54 Pt 1, 1–13 (1989).
3. Matzinger P Tolerance, danger, and the extended family. Annu Rev Immunol 12, 991–1045 (1994). [PubMed: 8011301]
4. Nathan C Points of control in inflammation. Nature 420, 846–852 (2002). [PubMed: 12490957]
5. Iwasaki A & Medzhitov R Regulation of adaptive immunity by the innate immune system. Science 327, 291–295 (2010). [PubMed: 20075244]
6. Zanoni I, Tan Y, Di Gioia M, Springstead JR & Kagan JC By Capturing Inflammatory Lipids Released from Dying Cells, the Receptor CD14 Induces Inflammasome-Dependent Phagocyte Hyperactivation. Immunity 47, 697–709 e693 (2017). [PubMed: 29045901]
7. Zanoni I et al. An endogenous caspase-11 ligand elicits interleukin-1 release from living dendritic cells. Science 352, 1232–1236 (2016). [PubMed: 27103670]
8. Imai Y et al. Identification of oxidative stress and Toll-like receptor 4 signaling as a key pathway of acute lung injury. Cell 133, 235–249 (2008). [PubMed: 18423196]
9. Shirey KA et al. The TLR4 antagonist Eritoran protects mice from lethal influenza infection. Nature 497, 498–502 (2013). [PubMed: 23636320]
10. Berliner JA, Leitinger N & Tsimikas S The role of oxidized phospholipids in atherosclerosis. J Lipid Res 50 Suppl, S207–212 (2009). [PubMed: 19059906]
11. Chang MK et al. Apoptotic cells with oxidation-specific epitopes are immunogenic and proinflammatory. J Exp Med 200, 1359–1370 (2004). [PubMed: 15583011]
12. Bochkov VN et al. Protective role of phospholipid oxidation products in endotoxin-induced tissue damage. Nature 419, 77–81 (2002). [PubMed: 12214235]
13. Leitinger N Oxidized phospholipids as modulators of inflammation in atherosclerosis. Curr Opin Lipidol 14, 421–430 (2003). [PubMed: 14501580]
14. Que X et al. Oxidized phospholipids are proinflammatory and proatherogenic in hypercholesterolaemic mice. Nature 558, 301–306 (2018). [PubMed: 29875409]
15. Dinarello CA Interleukin-1 in the pathogenesis and treatment of inflammatory diseases. Blood 117, 3720–3732 (2011). [PubMed: 21304099]
16. Jung J, Zeng H & Horng T Metabolism as a guiding force for immunity. Nature cell biology 21, 85–93 (2019). [PubMed: 30602764]
17. O'Neill LA & Pearce EJ Immunometabolism governs dendritic cell and macrophage function. J Exp Med 213, 15–23 (2016). [PubMed: 26694970]
18. Jha AK et al. Network integration of parallel metabolic and transcriptional data reveals metabolic modules that regulate macrophage polarization. Immunity 42, 419–430 (2015). [PubMed: 25786174]

19. Van den Bossche J et al. Mitochondrial Dysfunction Prevents Repolarization of Inflammatory Macrophages. Cell reports 17, 684–696 (2016). [PubMed: 27732846]
20. Serbulea V et al. Macrophage phenotype and bioenergetics are controlled by oxidized phospholipids identified in lean and obese adipose tissue. Proc Natl Acad Sci U S A 115, E6254–E6263 (2018). [PubMed: 29891687]
21. Everts B et al. TLR-driven early glycolytic reprogramming via the kinases TBK1-IKKvarepsilon supports the anabolic demands of dendritic cell activation. Nat Immunol 15, 323–332 (2014). [PubMed: 24562310]
22. Tannahill GM et al. Succinate is an inflammatory signal that induces IL-1beta through HIF-1alpha. Nature 496, 238–242 (2013). [PubMed: 23535595]
23. Palsson-McDermott EM et al. Pyruvate kinase M2 regulates Hif-1alpha activity and IL-1beta induction and is a critical determinant of the warburg effect in LPS-activated macrophages. Cell Metab 21, 65–80 (2015). [PubMed: 25565206]
24. Serbulea V et al. Macrophages sensing oxidized DAMPs reprogram their metabolism to support redox homeostasis and inflammation through a TLR2-Syk-ceramide dependent mechanism. Mol Metab 7, 23–34 (2018). [PubMed: 29153923]
25. Mills EL et al. Succinate Dehydrogenase Supports Metabolic Repurposing of Mitochondria to Drive Inflammatory Macrophages. Cell 167, 457–470 e413 (2016). [PubMed: 27667687]
26. Bailey JD et al. Nitric Oxide Modulates Metabolic Remodeling in Inflammatory Macrophages through TCA Cycle Regulation and Itaconate Accumulation. Cell reports 28, 218–230 e217 (2019). [PubMed: 31269442]
27. Meiser J et al. Pro-inflammatory Macrophages Sustain Pyruvate Oxidation through Pyruvate Dehydrogenase for the Synthesis of Itaconate and to Enable Cytokine Expression. J Biol Chem 291, 3932–3946 (2016). [PubMed: 26679997]
28. Wang F et al. Glycolytic Stimulation Is Not a Requirement for M2 Macrophage Differentiation. Cell Metab 28, 463–475 e464 (2018). [PubMed: 30184486]
29. Liu PS et al. alpha-ketoglutarate orchestrates macrophage activation through metabolic and epigenetic reprogramming. Nat Immunol 18, 985–994 (2017). [PubMed: 28714978]
30. Lampropoulou V et al. Itaconate Links Inhibition of Succinate Dehydrogenase with Macrophage Metabolic Remodeling and Regulation of Inflammation. Cell Metab 24, 158–166 (2016). [PubMed: 27374498]
31. Koivunen P et al. Inhibition of hypoxia-inducible factor (HIF) hydroxylases by citric acid cycle intermediates: possible links between cell metabolism and stabilization of HIF. J Biol Chem 282, 4524–4532 (2007). [PubMed: 17182618]
32. Ridker PM et al. Antiinflammatory Therapy with Canakinumab for Atherosclerotic Disease. The New England journal of medicine 377, 1119–1131 (2017). [PubMed: 28845751]
33. Koelwyn GJ, Corr EM, Erbay E & Moore KJ Regulation of macrophage immunometabolism in atherosclerosis. Nat Immunol 19, 526–537 (2018). [PubMed: 29777212]
34. Steinberg D & Witztum JL Oxidized low-density lipoprotein and atherosclerosis. Arterioscler Thromb Vasc Biol 30, 2311–2316 (2010). [PubMed: 21084697]
35. Oskolkova OV et al. Oxidized phospholipids are more potent antagonists of lipopolysaccharide than inducers of inflammation. J Immunol 185, 7706–7712 (2010). [PubMed: 21068406]
36. Kim K et al. Transcriptome Analysis Reveals Nonfoamy Rather Than Foamy Plaque Macrophages Are Proinflammatory in Atherosclerotic Murine Models. Circ Res 123, 1127–1142 (2018). [PubMed: 30359200]
37. Cochain C et al. Single-Cell RNA-Seq Reveals the Transcriptional Landscape and Heterogeneity of Aortic Macrophages in Murine Atherosclerosis. Circ Res 122, 1661–1674 (2018). [PubMed: 29545365]
38. Mahmood SS, Levy D, Vasan RS & Wang TJ The Framingham Heart Study and the epidemiology of cardiovascular disease: a historical perspective. Lancet 383, 999–1008 (2014). [PubMed: 24084292]
39. Sanin DE et al. Mitochondrial Membrane Potential Regulates Nuclear Gene Expression in Macrophages Exposed to Prostaglandin E2. Immunity 49, 1021–1033 e1026 (2018). [PubMed: 30566880]

40. Johnson MO et al. Distinct Regulation of Th17 and Th1 Cell Differentiation by Glutaminase-Dependent Metabolism. Cell 175, 1780–1795 e1719 (2018). [PubMed: 30392958]
41. Shirai T et al. The glycolytic enzyme PKM2 bridges metabolic and inflammatory dysfunction in coronary artery disease. J Exp Med 213, 337–354 (2016). [PubMed: 26926996]
42. Tavakoli S et al. Characterization of Macrophage Polarization States Using Combined Measurement of 2-Deoxyglucose and Glutamine Accumulation: Implications for Imaging of Atherosclerosis. Arterioscler Thromb Vasc Biol 37, 1840–1848 (2017). [PubMed: 28798141]
43. Hitzel J et al. Oxidized phospholipids regulate amino acid metabolism through MTHFD2 to facilitate nucleotide release in endothelial cells. Nat Commun 9, 2292 (2018). [PubMed: 29895827]
44. Bekkering S et al. Metabolic Induction of Trained Immunity through the Mevalonate Pathway. Cell 172, 135–146 e139 (2018). [PubMed: 29328908]
45. Christ A et al. Western Diet Triggers NLRP3-Dependent Innate Immune Reprogramming. Cell 172, 162–175 e114 (2018). [PubMed: 29328911]
46. Geng S et al. The persistence of low-grade inflammatory monocytes contributes to aggravated atherosclerosis. Nat Commun 7, 13436 (2016). [PubMed: 27824038]
47. Michelsen KS et al. Lack of Toll-like receptor 4 or myeloid differentiation factor 88 reduces atherosclerosis and alters plaque phenotype in mice deficient in apolipoprotein E. Proc Natl Acad Sci U S A 101, 10679–10684 (2004). [PubMed: 15249654]
48. Carnevale R et al. Localization of lipopolysaccharide from Escherichia Coli into human atherosclerotic plaque. Scientific reports 8, 3598 (2018). [PubMed: 29483584]
49. Philippova M et al. Analysis of fragmented oxidized phosphatidylcholines in human plasma using mass spectrometry: Comparison with immune assays. Free Radic Biol Med (2019).
50. Bjorkbacka H et al. Reduced atherosclerosis in MyD88-null mice links elevated serum cholesterol levels to activation of innate immunity signaling pathways. Nature medicine 10, 416–421 (2004).
51. Yuan M, Breitkopf SB, Yang X & Asara JM A positive/negative ion-switching, targeted mass spectrometry-based metabolomics platform for bodily fluids, cells, and fresh and fixed tissue. Nat Protoc 7, 872–881 (2012). [PubMed: 22498707]
52. Watson AD et al. Structural identification of a novel pro-inflammatory epoxyisoprostane phospholipid in mildly oxidized low density lipoprotein. J Biol Chem 274, 24787–24798 (1999). [PubMed: 10455151]
53. Yuan M et al. Ex vivo and in vivo stable isotope labelling of central carbon metabolism and related pathways with analysis by LC-MS/MS. Nat Protoc 14, 313–330 (2019). [PubMed: 30683937]
54. Kannel WB, Feinleib M, McNamara PM, Garrison RJ & Castelli WP An investigation of coronary heart disease in families. The Framingham offspring study. Am J Epidemiol 110, 281–290 (1979). [PubMed: 474565]
55. Joehanes R et al. Gene expression signatures of coronary heart disease. Arterioscler Thromb Vasc Biol 33, 1418–1426 (2013). [PubMed: 23539218]
56. Irizarry RA et al. Exploration, normalization, and summaries of high density oligonucleotide array probe level data. Biostatistics 4, 249–264 (2003). [PubMed: 12925520]
57. Joehanes R et al. Integrated genome-wide analysis of expression quantitative trait loci aids interpretation of genomic association studies. Genome Biol 18, 16 (2017). [PubMed: 28122634]

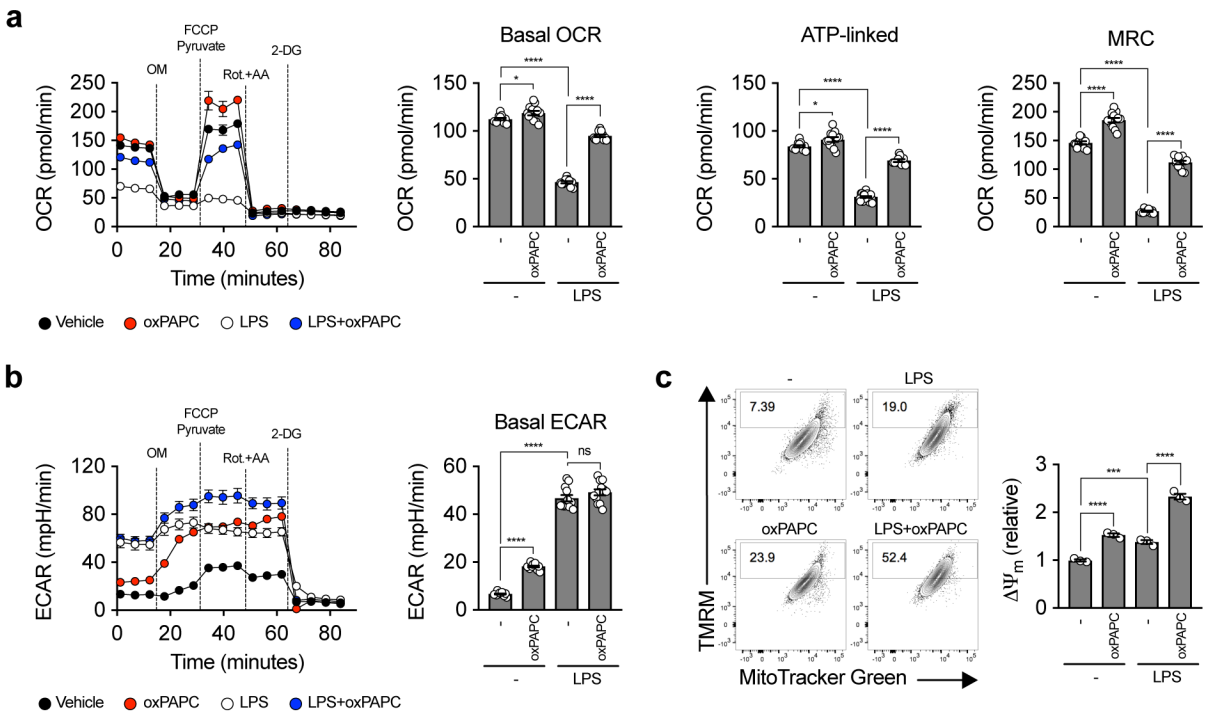

Figure 1. oxPAPC induces a hypermetabolic state in macrophages

a, b) Bone marrow-derived macrophages (BMDMs) were primed or not with LPS (1 μg/ml) for 3 hours and then stimulated with oxPAPC (100 μg/ml) for 24h. OCR (**a**) (left panels: kinetic line graph; right panels: basal OCR, ATP-linked respiration and MRC bar graphs) and ECAR (**b**) (left panel: kinetic line graph; right panel: basal ECAR bar graph) were measured using a Seahorse Analyzer.

c) BMDMs were treated as in (**a, b**) and $\Delta\psi_m$ was assessed by cytofluorimetry. Left panels: cytofluorimetry contour plot, right panel: bar graph. $\Delta\psi_m$ is calculated as the ratio between the fluorescent intensity of TMRM and the fluorescent intensity of mitochondrial mass (MitoTracker Green). Bars represent the $\Delta\psi_m$ of cells treated as indicated relative to untreated cells.

Graphs and images are representative of one out of three independent experiments. Graphs show mean ± s.e.m. of twelve (a-b) or three (c) biological samples. Statistical comparisons were calculated by using two-way ANOVA (*$P < 0.05$, **$P < 0.01$, ***$P < 0.001$ and ****$P < 0.0001$).

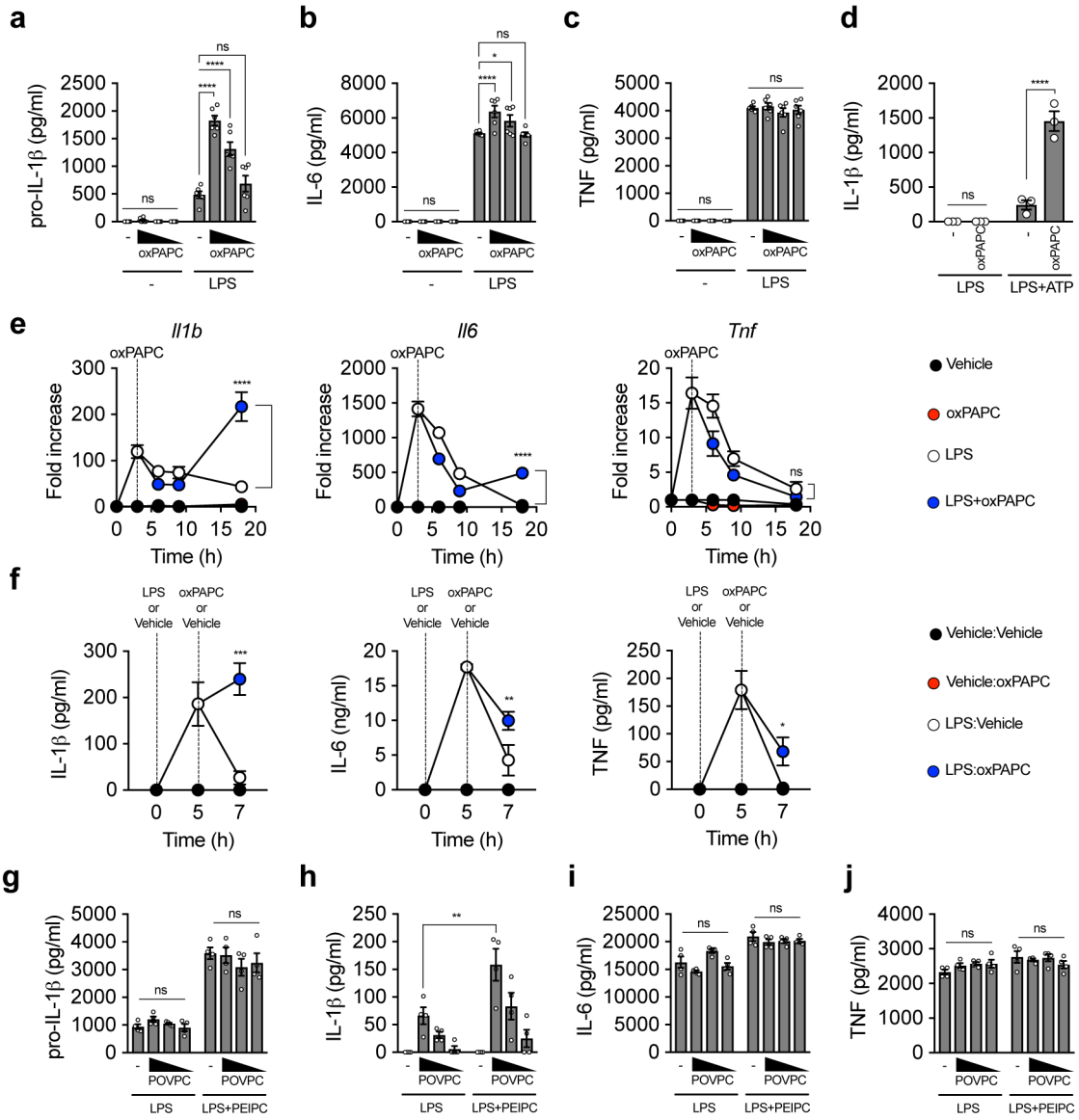

Figure 2. oxPAPC promotes a hyperinflammatory phenotype in LPS-stimulated macrophages.

a-c) BMDMs were primed or not with LPS and then treated, or not, with oxPAPC (100, 50 and 25 μg/ml). Indicated cytokines were quantified 24h later from cell lysate (pro-IL-1β) (**a**) or from supernatant (IL-6, TNF) (**b, c**).

d) BMDMs were primed or not with LPS and then treated, or not, with oxPAPC (100 μg/ml) for 24h. Cells were then administered or not with ATP (3 mM) and 6h later the amount of IL-1β released in the supernatant was measured.

e) BMDMs were primed or not with LPS and then treated, or not, with oxPAPC (100 μg/ml). Indicated mRNA was measured at the indicated time points.

f) Mice (n=5) were injected with LPS (1mg/Kg) or vehicle (PBS) for 5h and then challenged, or not, with oxPAPC (80mg/Kg). Blood serum was collected 2h after oxPAPC administration and IL-1β, IL-6 and TNF were quantified.

g-j) BMDMs were primed with LPS and then treated, or not, with PEIPC (50 μM) and/or POVPC (100, 50 and 25 μM). Indicated cytokines were quantified 24h later from cell lysate (pro-IL-1β) (**g**) or from supernatant (IL-1β, IL-6, TNF) (**h-j**).
Graphs are representative of one out of three (a-e) or two (g-j) independent experiments. Graphs show mean ± s.e.m. of six (a-c), three (d-e) or four (g-j) biological samples. Statistical comparisons were calculated by using two-way ANOVA (a-e, g-j) or two-tailed *t* test (f) (**P* < 0.05, ***P* < 0.01, ****P* < 0,001 and *****P* < 0,0001).

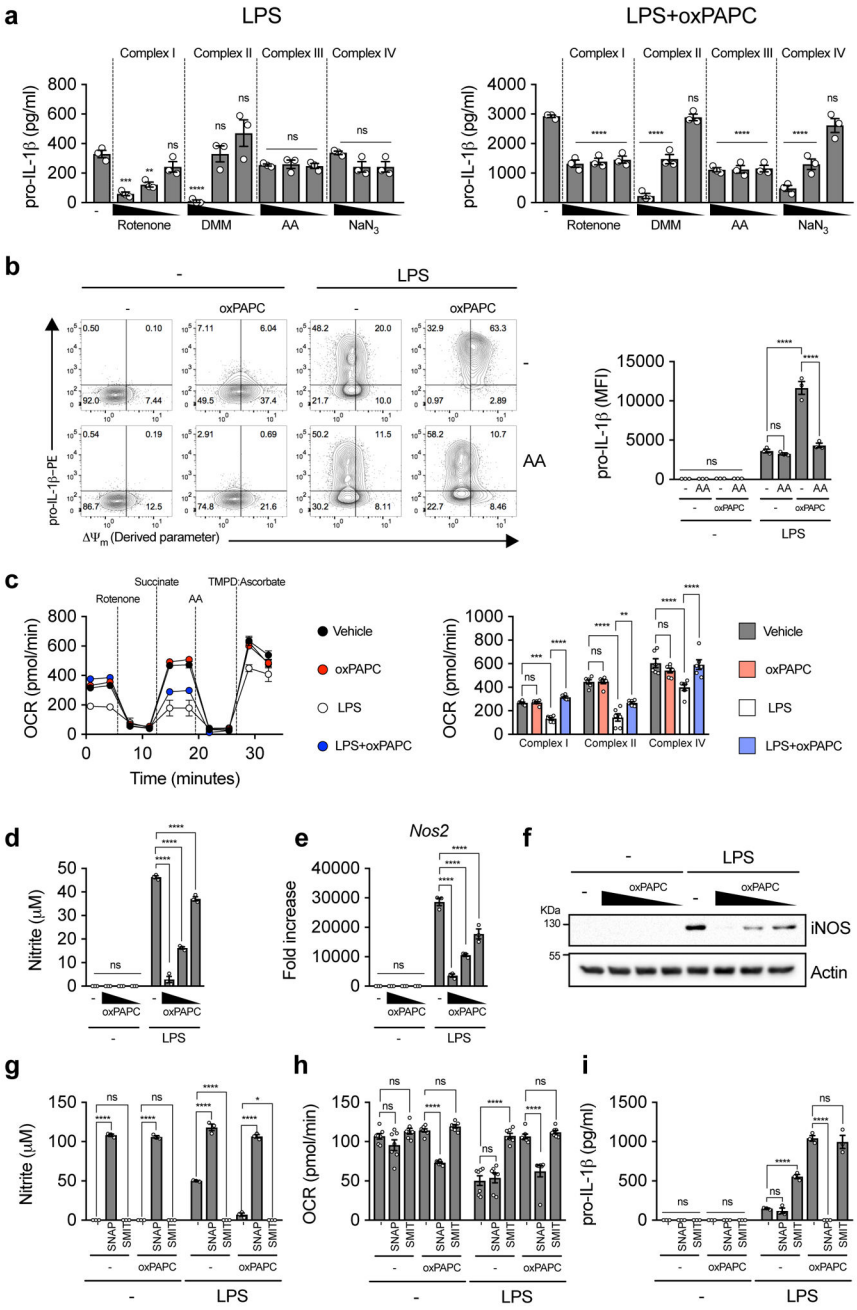

Figure 3. Nitric oxide inhibition and respiration maintenance promoted by oxPAPC enables the hyperproduction of IL-1β.

a) BMDMs were primed with LPS and then stimulated, or not, with oxPAPC (100 μg/ml) in the presence or absence of rotenone (10, 1, 0.1 μM), dimethyl malonate (DMM) (10, 5, 2.5 μM), antimycin A (AA) (5, 2.5, 1.25 μM) or sodium azide (NaN_3) (200, 20, 2 μM). Pro-IL-1β was measured 24 hours later.

b) BMDMs were primed or not with LPS and then stimulated with oxPAPC (100 μg/ml) in the presence or absence of AA (5 μM). Pro-IL-1β and $\Delta\psi_m$ were measured by cytofluorimetric intracellular staining. Left panels: cytofluorimetry contour plot, right panel: bar graph. Bars represent the mean fluorescence intensity (MFI) of pro-IL-1β staining.

c) BMDMs were primed, or not, with LPS and then stimulated, or not, with oxPAPC (100 μg/ml) for 24h. The electron flow activity through the different complexes of ETC was analyzed in permeabilized cells using the indicated inhibitors or substrates. Left panel: line graph; right panel: bar graph.

d-f) BMDMs were primed, or not, with LPS and then stimulated, or not, with oxPAPC (100, 50 and 25 μg/ml). 24h later nitrite concentration (**d**), *Nos*2 mRNA(**e**), and iNOS protein (**f**) were analyzed.

g-i) BMDMs were primed, or not, with LPS and then stimulated, or not, with oxPAPC (100 μg/ml) in the presence or absence of either SNAP (500 μM) or SMIT (500 μM). Nitrate production (**g**) was measured 24h later. Basal OCR (**h**) was analyzed, and pro-IL-1β **(i**) was measured from cell lysate.

Graphs are representative of one out of two (a), three (b-c, e-i) or ten (d) independent experiments. Graphs show mean ± s.e.m. of three (a-b, d-g, i), six (c) or seven (h) biological samples. Statistical comparisons were calculated by using two-way ANOVA (*$P < 0.05$, **$P < 0.01$, ***$P <$ 0,001 and ****$P <$ 0,0001).

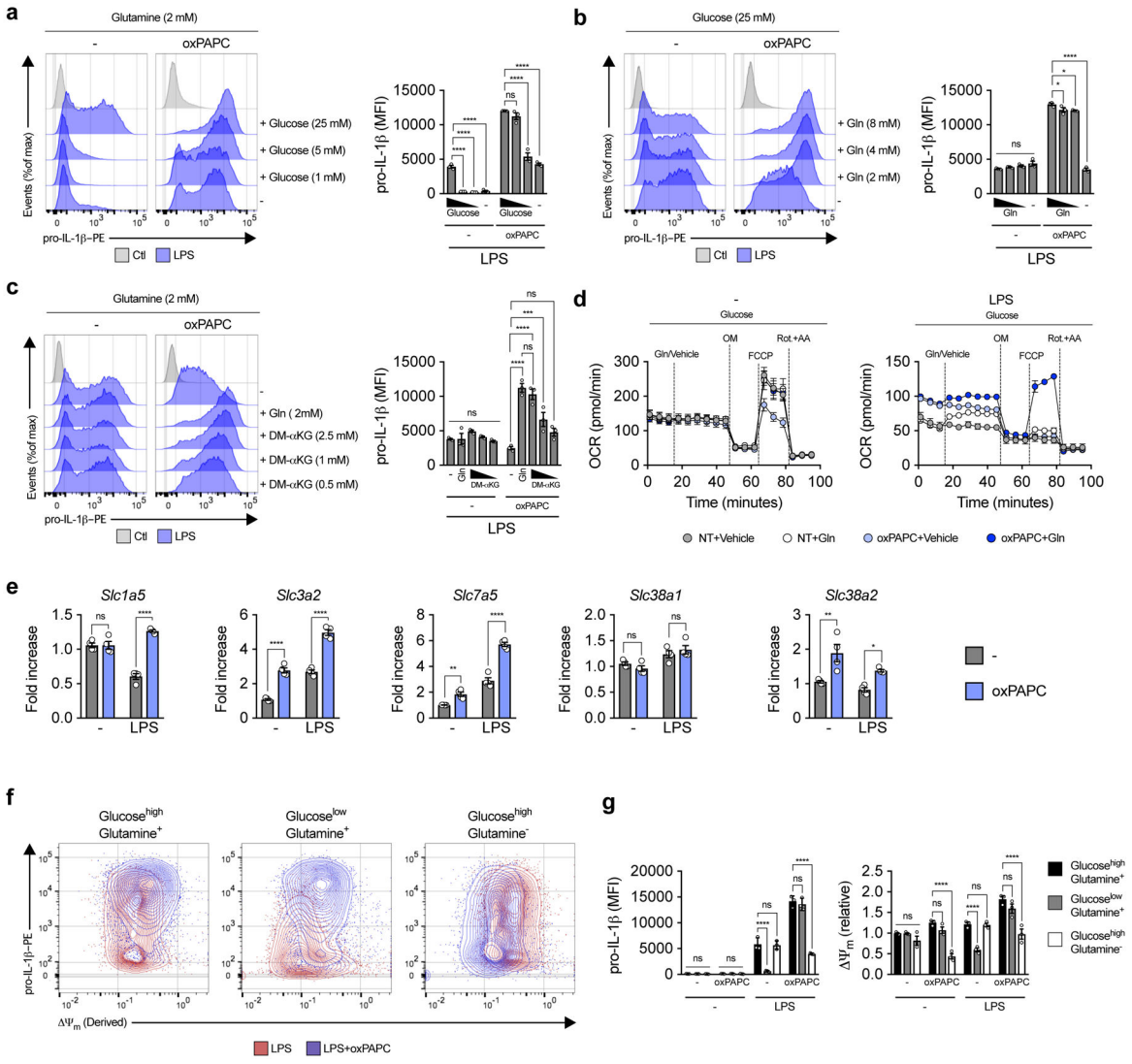

Figure 4. Glutamine is strictly required for oxPAPC-mediated hyperinflammation

a-c) BMDMs were primed or not with LPS and then stimulated with oxPAPC (100 μg/ml) for 24h in a medium containing the indicated carbon sources. pro-IL-1β was measured by cytofluorimetric intracellular staining. Left panels: cytofluorimetry histograms, right panel: bar graph. Bars represent the mean fluorescence intensity (MFI) of pro-IL-1β. Ctl: Vehicle-treated cells; Gln: glutamine; DM-αKG: dimethyl α-ketoglutarate.

d) BMDMs were primed (right panel) or not (left panel) with LPS and then stimulated with oxPAPC (100 μg/ml) for 24h. OCR was measured under glutamine deprivation (25 mM glucose as the only substrate in the medium) or after glutamine (2mM) injection using a Seahorse Analyzer. Gln: glutamine; NT: not treated.

e) BMDMs were primed or not with LPS and then stimulated, or not, with oxPAPC (100 μg/ml). The transcription of the indicated glutamine transporters was measured 24h later.

f, g) BMDMs were primed or not with LPS and then stimulated with oxPAPC (100 μg/ml) for 24h in a medium containing the indicated carbon sources ($Glucose^{high}$=25mM; $Glucose^{low}$=5mM $Glutamine^{+}$=2mM; $Glutamine^{-}$=0mM). Pro-IL-1β and $\Delta\psi_m$ were

measured by cytofluorimetric intracellular staining. Cytofluorimetry contour plot (**f**) and bars that represent the mean fluorescence intensity (MFI) of pro-IL-1β or $\Delta\psi_m$ (**g**) are shown.

Graphs are representative of one out of four (a-d, f-g) or three (e) independent experiments. Graphs show mean ± s.e.m. of three (a-c, f-g) four (e) or six (d) biological samples. Statistical comparisons were calculated by using two-way ANOVA (*$P < 0.05$, **$P < 0.01$, ***$P < 0.001$ and ****$P < 0.0001$).

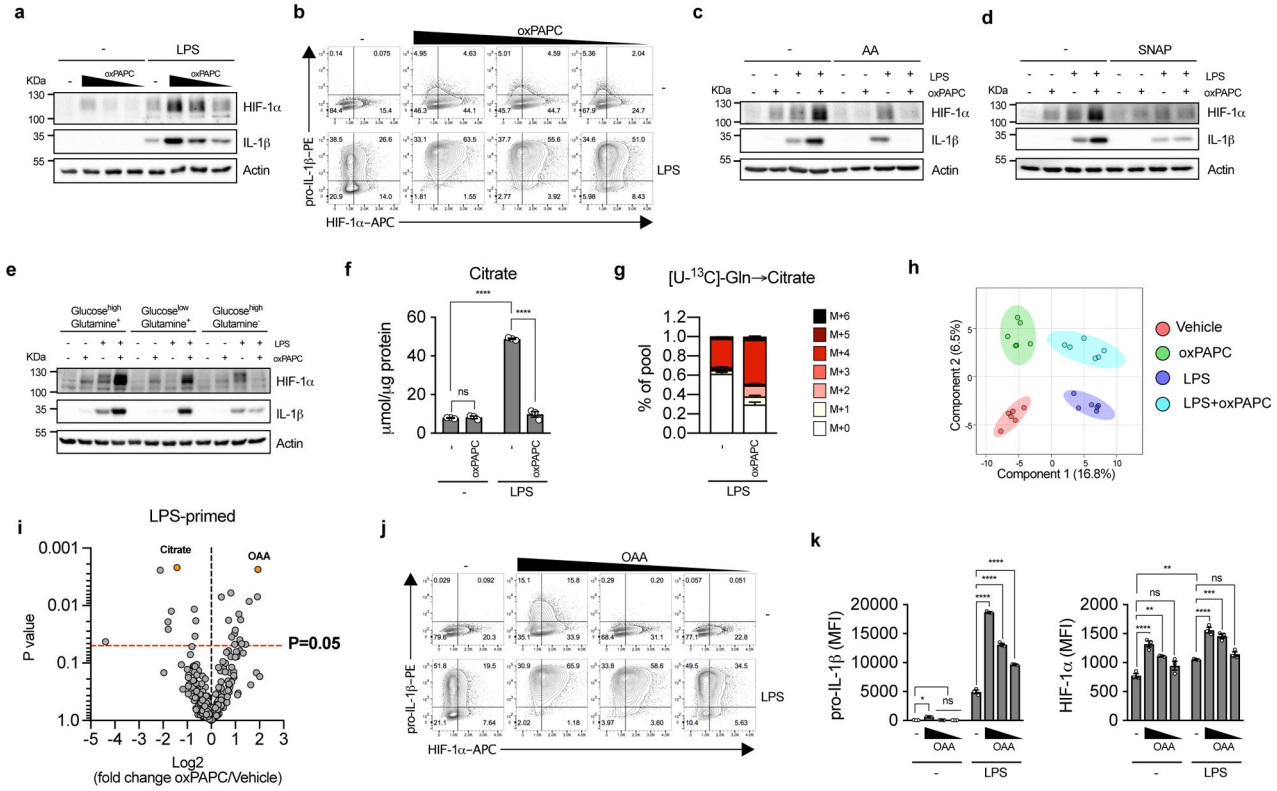

Figure 5. oxPAPC potentiates HIF-1α through oxaloacetate accumulation

a, b) Immunoblot (**a**) and cytofluorimetry (**b**) measurement of HIF-1α and IL-1β protein levels after 24h of oxPAPC treatment (100, 50 and 25 µg/ml) in BMDMs primed, or not, with LPS.

c-e) Immunoblot measurement of HIF-1α and IL-1β protein levels after 24h of oxPAPC treatment (100 µg/ml) in BMDMs primed, or not, with LPS cultured in a medium containing Antymicin A (AA) (5 µM) (**c**), SNAP (500 µM) (**d**), or the carbon sources indicated in Fig. 4f, g (**e**).

f) BMDMs primed with LPS and treated, or not, with oxPAPC (100 µg/ml). Citrate levels were quantified from cell lysates by fluorescence and normalized for the protein content.

g) BMDMs primed with LPS were treated, or not, with oxPAPC (100 µg/ml). 24 hours later, cells were incubated with [U-^{13}C]-glutamine for 4h. The percentage of M+0 to M+6 citrate is shown.

h, i) BMDMs primed with LPS were treated, or not, with oxPAPC (100 µg/ml). 24 hours later, a metabolomics analysis was performed. The sparse Partial Least Squares Discriminant Analysis (sPLS-DA) two-dimensional scores plot (**h**) and the volcano plot (**i**) are shown. Oxaloacetate (OAA) and citrate are highlighted in orange (n=6 independent experiments).

j, k) Pro-IL-1β and HIF-1α protein levels were measured by cytofluorimetry in BMDMs primed, or not, with LPS and treated, or not, with oxaloacetate (OAA) (50, 25, 12.5 mM). Cytofluorimetry contour plot (**j**) and bars represent the mean fluorescence intensity (MFI) of pro-IL-1β (left) and HIF-1α (right) (**k**) are shown.

Graphs and images are representative of one out of three (a-g, j-k) independent experiments. Graphs show means ± s.e.m. of three (f, g, k) biological replicates. Statistical comparisons

were calculated by using two-way ANOVA (*$P < 0.05$, **$P < 0.01$, ***$P < 0.001$ and ****$P < 0.0001$).

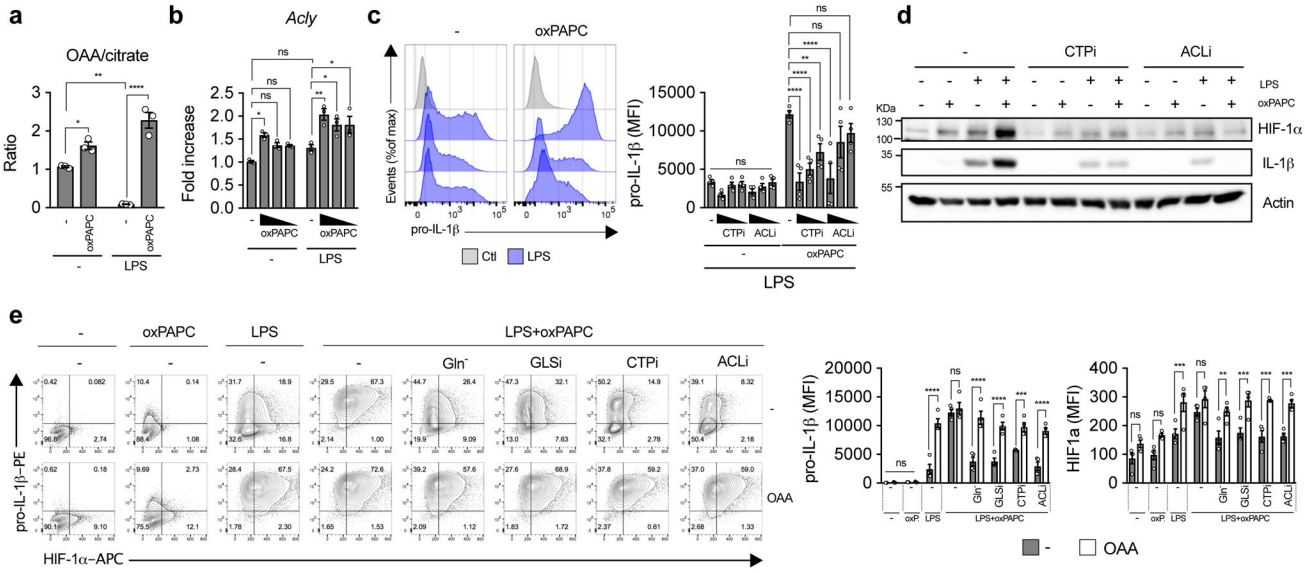

Figure 6. The conversion of citrate into oxaloacetate in the cytoplasm governs the induction of the hyperinflammatory phenotype in macrophages treated with oxPAPC and LPS.

a) BMDMs primed with LPS were treated, or not, with oxPAPC (100 μg/ml). 24 hours later, the citrate and oxaloacetate levels were quantified from cell lysates by fluorescence and normalized for the protein content. Ratio normalized on untreated cells is shown. OAA: oxaloacetate.

b) BMDMs primed with LPS were treated, or not, with oxPAPC (100 μg/ml). 24 hours later the levels of *Acly* mRNA were assessed.

c, d) BMDMs primed, or not, with LPS were treated, or not, with oxPAPC (100 μg/ml) in the presence, or absence, of CTPi (0.5, 0.2 and 0.1 mM in **c**, 1 mM in **d**) or ACL inhibitor BMS-303141 (ACLi) (30, 15 and 7.5 μM in **c**, 30 μM in **d**). 24 hours after LPS administration, pro-IL-1β was quantified by flow cytometry (**c**) (left panel: histogram; right panel: bar graph) and pro-IL-1β or HIF-1α protein levels were measured by immunoblotting (**d**).

e) BMDMs primed, or not, with LPS were treated, or not, with oxPAPC (100 μg/ml) in a medium containing or not glutamine (Gln-), and in the presence, or absence, of CB-839 (GLSi) (1 μM), CTPi (0.5 mM) and ACLi (30 μM). All treatments were performed in presence, or absence (−), of oxaloacetate (25mM). pro-IL-1β (left) and HIF-1α were measured by cytofluorimetry. Left panel: cytofluorimetry contour plot; right panels: graph bars (mean fluorescence intensity, MFI).

Graphs and images are representative of one out of three (a, b) or two (c-e) independent experiments. Graphs show mean ± s.e.m. of three (a, b) or four (c, e) biological replicates. Statistical comparisons were calculated by using two-way ANOVA (*$P < 0.05$, **$P < 0.01$, ***$P < 0.001$ and ****$P < 0.0001$).

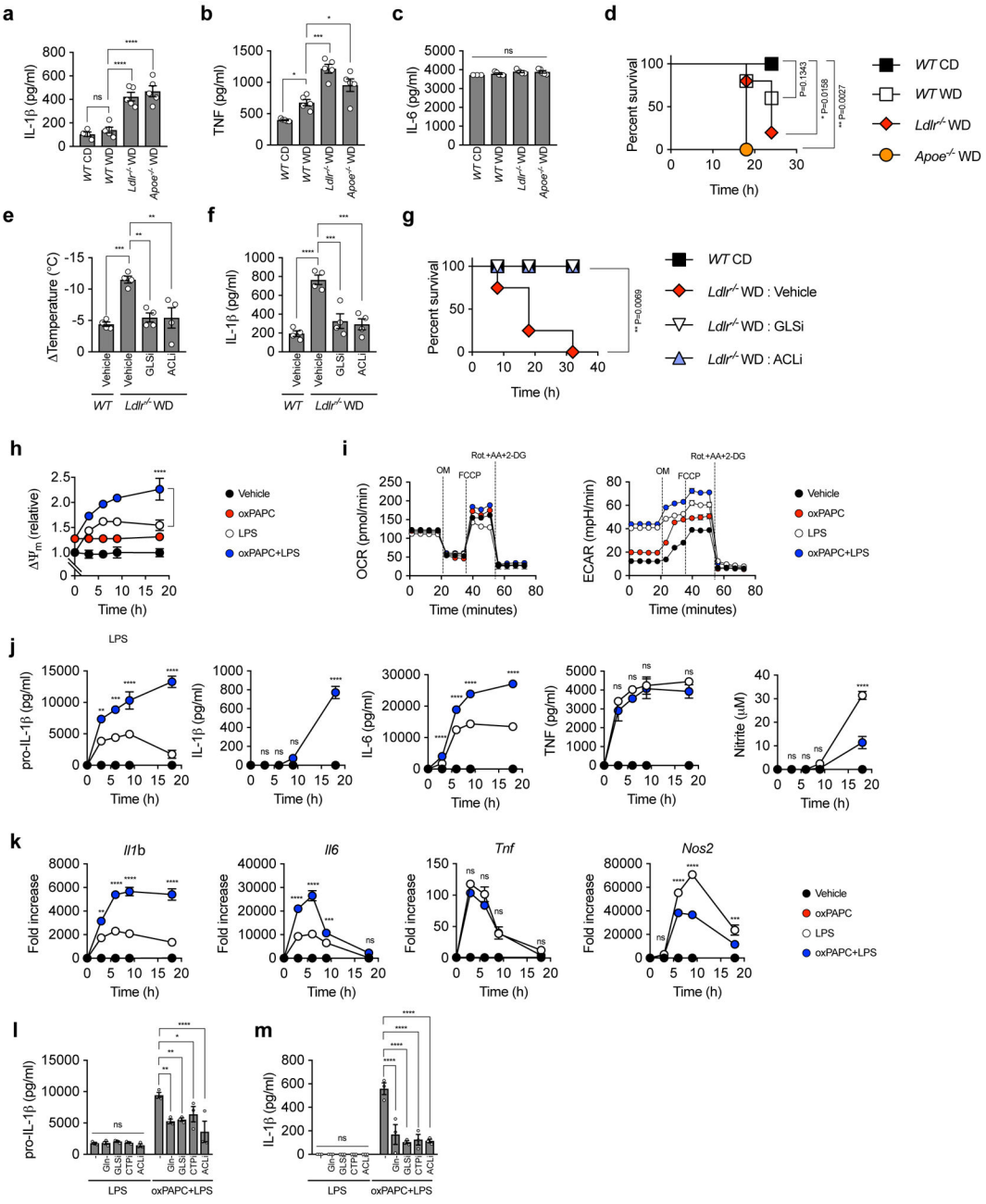

Figure 7. oxPAPC-driven immunometabolic adaptations occur in hypercholesterolemic mice.

a-g) Wild type (*WT*), *Ldlr*$^{-/-}$ and *Apoe*$^{-/-}$ mice (n=5) were fed a western diet (WD) for 4 weeks. As control, *WT* mice were also fed a conventional diet (CD). Mice (n=6) were injected with LPS (1 mg/Kg) and *Ldlr*$^{-/-}$ mice were also treated, or not, with GLSi or ACLi 1 hour before LPS injection. Serum levels of IL-1β (**a, f**), TNF (**b**) and IL-6 (**c**) were 5h later. Body temperature loss was measured 8h later (**e**) and survival was followed over time (**d, g**).

h-m) BMDMs were treated, or not, with oxPAPC (100 μg/ml) for 24 hours and activated, or not, with LPS (1 μg/ml). In some experiments, cells were cultured in the absence of glutamine (Gln-) or in the presence of GLSi (1 μM), CTPi 0.5 mM) or ACLi (30 μM). $\Delta\psi_m$

was assessed by cytofluorimetry at the indicated time points after LPS administration (**h**). The indicated metabolic parameters (**i**) were measured 8h after LPS administration. At the indicated time points after LPS administration, the indicated cytokines were quantified either by ELISA (pro-IL-1β from cell lysate; IL-1β, TNF, IL-6 from supernatant) (**j**) or by qPCR (**k**), while nitrite concentration was measured using Greiss reagent (**j**) and iNOS mRNA levels were measured by qPCR (**k**). pro-IL-1β from cell lysate and secreted IL-1β from supernatant were measured 18h after LPS administration (**l**,**m**).

Graphs and images are representative of one out of three (h-k) or two (l, m) independent experiments. Graphs show mean ± s.e.m. of three (h, j-m) or six (i) biological samples. Statistical comparisons were calculated by using one-way ANOVA (a-c, e-f), two-way ANOVA (h, j-m) and Long-rank test with Bonferroni correction (d, g). (*$P < 0.05$, **$P < 0.01$, ***$P < 0.001$ and ****$P < 0.0001$).

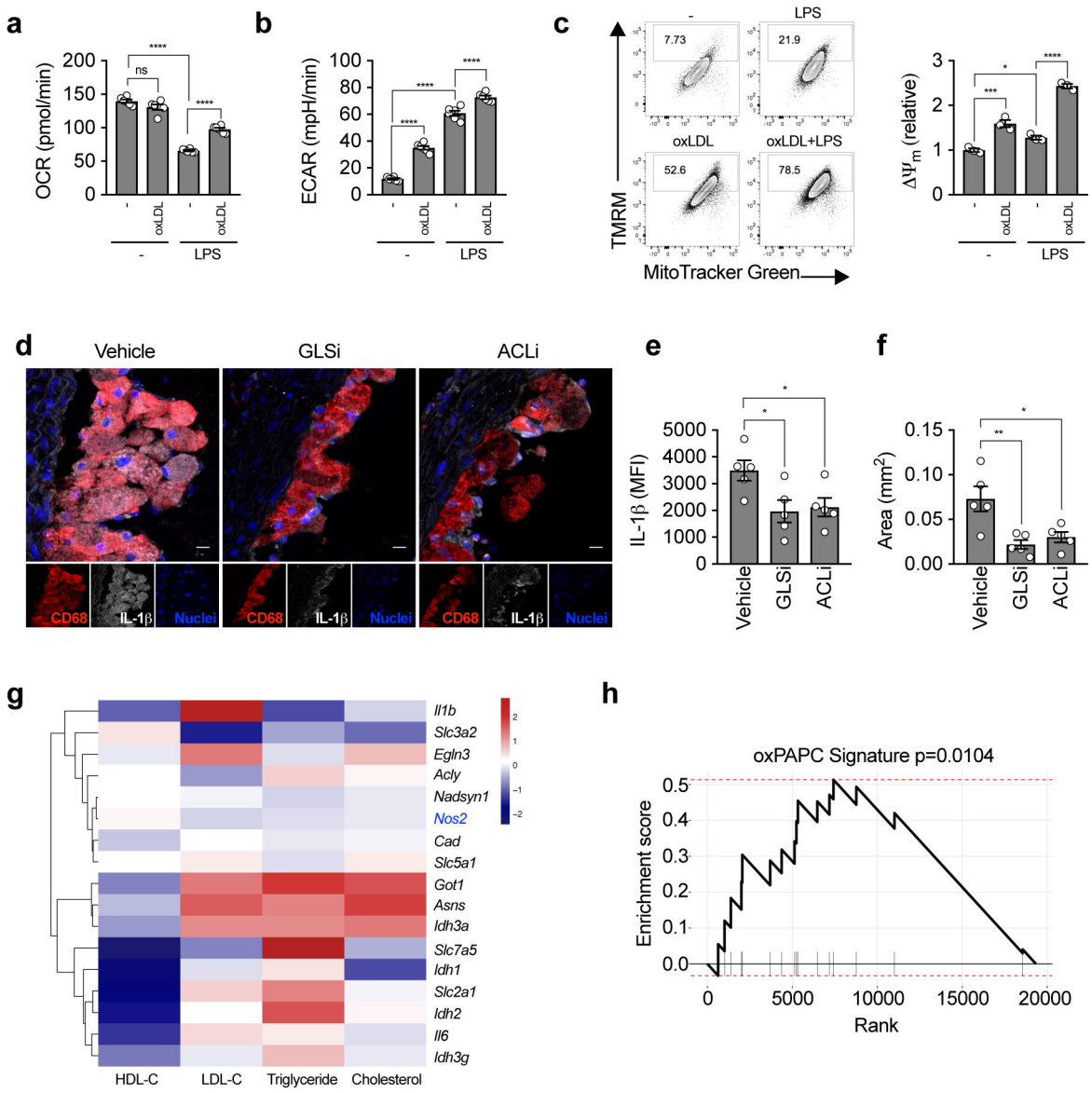

Figure 8. The hypermetabolism induced by oxidized phospholipids can be targeted against atherosclerosis.

a-c) oxLDL-treated BMDMs (oxLDL) or naïve BMDMs (−) were treated or not with LPS and 24 hours later OCR (**a**), ECAR (**b**) and $\Delta\psi_m$ (**c**) were measured

d-f) *Ldlr*$^{-/-}$ mice (n=5) were fed a WD for 4 weeks and treated, or not, with GLSi (12.5 mg/Kg) or ACLi (10 mg/Kg) three times/week. IL-1β (**d, e**) was quantified as mean of fluorescence intensity in CD68-positive cells from aortic plaques. Lesion areas (**f**) were quantified using Oil Red O (ORO) and hematoxylin staining. Scale bar: 10 μm.

g, h) Heat map of standardized gene coefficients in linear regression for HDL-C, LDL-C, Triglycerides or Total Cholesterol (Cholesterol). The set of genes upregulated by oxPAPC in mouse, plus (downregulated) *Nos2* (in blue), are shown (**g**). Gene Set Enrichment Analysis p-value and enrichment plot of the oxPAPC signature against genes ranked by association

with pro-atherosclerotic lipids in the FHS cohort (**h**) support that oxPAPC-induced genes identified in mouse show consistent expression patterns in humans.
Graphs and images are representative of one out of three (a-c) independent experiments. Graphs show mean ± s.e.m. of six (a, b) or three (c) biological samples. Statistical comparisons were calculated by using two-way ANOVA (a-c) or one-way ANOVA (e, f) (*$P < 0.05$, **$P < 0.01$, ***$P < 0.001$ and ****$P < 0.0001$).